République Algérienne Démocratique et Populaire
Ministère de l'Enseignement Supérieur
et de la Recherche Scientifique
Université de Tissemsilt

Faculté des Sciences et de la Technologie
Département des Sciences de la Matière

Mémoire de fin d'études pour l'obtention du diplôme
de Master académique en

Filière :**Physique**

Spécialité : **nano-physique**

Présentée par : **GHAROU AHMED**

Thème

Electric properties simulation of nano-crystalline silicon solar cells

---

Soutenu le 01/06/2023

Devant le Jury :

CHAKER Yassine	Président	M.C.A.	Univ-Tissemsilt
CHAHI Mokhtar	Encadreur	M.C.B.	ESGEE-Oran
BOUHEKKA Ahmed	Co-Encadreur	Prof.	Univ-Tissemsilt
BOUDIA Kaltouma	Examinatrice	Prof.	Univ-Tissemsilt

Année universitaire : 2022-2023

Abstract

The main objective of this master project is to simulate the transport properties in nanocrystalline thin films for solar cells applications using a program wxAMPS. To achieve this goal, we built a layer of nanocrystalline silicon based on successive layer by layer of crystalline and amorphous small layer. Then we generate the calculation for different samples of different thicknesses. The activation energy of all the simulated samples was calculated and compared to experimental previous works. A good agreement between theory and experiment was observed and the activation energy for doped material is lower than un-doped ones.

Keywords

Nanocrystalline silicon, solar cells, doped materials, activation energy.

Résumé

L'objectif principal de ce projet de master est de simuler les propriétés de transport dans des couches minces à base de silicium nanocristallin pour des applications de cellules solaires à l'aide d'un programme wxAMPS . Pour atteindre cet objectif, nous avons construit une couche de silicium nanocristallin à base des couches minces successives du silicium cristal et amorphe. Ensuite, nous générons le calcul pour différents échantillons d'épaisseurs différentes. L'énergie d'activation de tous les échantillons simulés a été calculée et comparée à des travaux expérimentaux antérieurs. Un bon accord entre la théorie et l'expérience a été observé et l'énergie d'activation pour les matériaux dopés est inférieure à celle des matériaux non dopés.

Mots clés

Silicium nanocristallin, cellules solaires, matériaux dopés, énergie d'activation .

ملخص

الهدف الرئيسي لهذا المشروع هو محاكاة خصائص النقل الالكتروني في الأغشية الرقيقة البلورية الدقيقة لتطبيقات الخلايا الشمسية باستخدام برنامجwxAMPS و ذلك من اجل تطبيقها في خلايا الطاقة الشمسية.

لتحقيق هذا الهدف، قمنا ببناء طبقة سيليكون بلورية دقيقة تعتمد على طبقات متتالية من السيليسيوم البلوري و غير البلوري. ثم نقوم بتوليد الحساب على عينات مختلفة السمك. بالاعتماد على نتائج الحساب نقوم باستخراج طاقة التنشيط من المنحنيات الممثلة لخاصية الكثافة الكهربائية فرق الكمون و العمل على مقارنتها بالعمل التجريبي.

من خلال المقارنة لوحظ تطابق جيد بين نتائج المحاكاة و نتائج التجارب و لوحظ كذلك أن طاقة التنشيط في الأغشية ذات التطعيم P اقل من الأغشية عديمة التطعيم .

الكلمات الرئيسية

سيليكون نانو كريستالين،خلايا شمسية،مواد تطعيم ،طاقة تنشيط .

Acknowledgments

Praise is to Allah who enabled me to finish my scientific work.

I would like to thank Dr. Chahi Mokhtar and Prof. Bouhekka Ahmed for supervising my master project and for all scientific meetings and discussions with them, and I thank them for their professionalism and discipline in their work. I am very happy and proud of this chance that I got to work with them..

I would like to thank the president of the jury Dr. Chaker Yassine and the examiner Prof. Boudia Kaltouma for their time and in advance for their scientific comments and critics that will improve this manuscript. I would like to thank all the teachers who formed and taught me and led me through my primary academic career to university.

I would like to dedicate this work to my father and mother and brothers, I want to thank them for everything they have given me of moral and physical support , and I hope you will be proud of me and of this work.

I would like to thank everyone who supported me for this work, and also extend my greetings to my friends and all my colleagues who studied with me, and I am sorry that I cannot mention all of you

I wish to you all the best and success in your future plans.

Ahmed,

List of figures

Chapter 1

Figure 1. The Relationship among cell, module and array **18**

Figure 2. The structure of solar cell..... **18**

Figure 3. Schematic structure diagrams of a) crystalline silicon and b) corresponding energy bands..... **20**

Figure 4. Schematic structure diagrams of amorphous silicon, and hydrogenated.. **21**

Figure 5. State density of a- crystalline, b-amorphous and hydrogenated amorphous silicon **22**

Figure 6. Names of different structure according to the size of crystallites **24**

Figure 7. Microcrystalline silicon structure **24**

Figure 8. The distribution of defects as indicated by Seto model and homogenous one **27**

Figure 9. Schematic representation of a- the surface model and b-growth zone model for nc -Si:H..... **27**

Figure 10. The morphology of microcrystalline silicon **29**

Figure 11. Reactions between plasma and substrate surface **30**

Figure 12. Energy-band diagram for a p-n homojunction with equal densities of doping in the p- and n-type portions **31**

Figure 13. Energy-band diagram for a p-n homojunction with equal densities of doping in the p- and n-type portions, and a choice of material parameters ($\chi_1 < \chi_2$, $E_{G1} < E_{G2}$) such that the are no energy spikes at the junction interface **31**

Chapter 2

Figure 1. Schematic model simulation: (A) nc-Si constituted by crystalline region (nanocrystallites) and amorphous region (grain boundaries). (B) Simulation following the Seto and Lecomber models **..... 40**

Figure 2. Band diagram of nano-crystalline silicon (A) in thermodynamic equilibrium and (B) in non thermodynamic equilibrium **..... 45**

Figure 3. Current density voltage characteristics of nanocrystalline silicon under dark conditions at different temperature values (*Ln(current density)* indicated in right figure **..... 46**

Figure 4. An example of n30min sample illustrating fitting procedure to determine the activation energy of the samples **..... 47**

Figure 5. Simulated variation of $LogJ_0(T)$ as a function of the inverse of KT **..... 48**

Figure 6. Simulated variation of $LogJ_0(T)$ as a function of the inverse of KT **..... 49**

Figure 7. Simulated variation of $LogJ_0(T)$ as a function of the inverse of KT **..... 50**

Figure 8. Diagram of the VRH hopping processes that account for electric transport in semiconductor materials for the region of low temperature. R_H and W_H indicate range and energy hopping activation**..... 51**

Figure 9. The variation of simulated $LogJ_0(T)$ as a function of $T^{-0.25}$ for all the samples deposited during 3 min and 30 min at T = 100°C **..... 52**

Figure 10. Variation, as a function of ($T_0^{0,25}$), of $N(E_F)$ obtained for the samples. Continues line used to guide the eye**..... 54**

Figure 11. Variation, as a function of T, of the average hopping distance R_h. **..... 55**

Figure 12. Variation, as a function of T, of the hopping energy deduced using the VRH model, for selected films deposited at 100°C, during 3 min and 30 min **..... 56**

Figure 13. Simulated variation of $LogJ_0(T)$ as a function of the inverse of KT **..... 58**

List of tables

Table1. Magnitude order of mobility of holes and electrons at room temperature **.. 26**

Table 1. Summarizing simulated and experimental values of the disorder parameter T_0 and N(E_F)**..... 53**

Table 2. Summarizing simulated and experimental values of R_h and W_h obtained at room temperature **..... 57**

Table of contents

Abstract ..... **ii**

Acknowledgments ..... **v**

List of figures ..... **vi**

List of tables ..... **vii**

Table of contents ..... **ix**

General introduction **11**

CHAPTER I GENERALITIES ABOUT SILICON

1. **Introduction** **17**
2. **The need for solar energy (photovoltaic PV)** **17**

2.1. The role of silicon thin films in PV **19**

3. **Different structures of silicon** **19**

3.1 Crystalline silicon **19**

3.2 Amorphous silicon **20**

3.3 Polycrystalline silicon **22**

3.4 Microcrystalline silicon **23**

3.5 Nanocrystalline silicon nc-S **23**

4. **Electrical properties of microcrystalline silicon** **24**

4.1 Conductivity **24**

a. **The pre-exponential factor of conductivity** **25**

b. **Activation energy** **25**

c. **Coplanar and transversal conductivity** **25**

4.2 Mobility **26**

4.3 Transport in nc-Si **26**

4.4 Models of transport of charge **26**

a. **Adapted Seto Model** **27**

b. **Homogenous Model** **27**

5. **Growth model of nc-Si:H** **28**
6. **Plasma-substrate interactions** **29**

a. **Homojunctions** **30**

b. **Heterojunctions** **31**

7. **Conclusion** **32**
8. **REFERENCES** **33**

Chapter II wxAMPS Simulation of Electrical Properties of nc-Si:H: Model and Results

1. Introduction 37
2. wxAMPS simulation tool 37
   2.1. Carrier Transport in Semiconductors 37
   2.1.1. The transport equations 38
   2.1.2. Continuity equations 38
   2.1.3. Poisson's Equation 39
3. Simulation model 40
   3.1 Simulation Parameters 41
4. Results and discussion 41
   4.1. Diagram band structure 45
   4.1.1. Transport mechanisms 45
   4.1.2. Current-voltage characteristic 46
   4.1.2.1. Activation energy conductivity 46
   4.2. Intrinsic μc-Si:H 47
   4.3. n doped μc-Si:H 49
   4.4. p doped μc-Si:H 49
   4.5. Hopping parameters 50
   4.5.1. N (E_F) parameter 52
   4.5.2. Range hopping R_H 54
   4.5.3. Energy range hopping W_h 55
   4.6. Crystalline fraction effect on activation energy 57
5. Conclusion 58
6. REFERENCES 60
7. General Conclusion 6

General Introduction

In the last years the demand of energy and the consummation is increasing very fast because the population of the world is increasing too plus the industry and other sectors that need this important key factor of life. The need for new resources of energy is mandatory that is why solar cells or photovoltaic attracted researchers because it is considered as the most strategically solutions that can help humanity to across this difficult stage of energy need.

Photovoltaic is based on the principal of transforming sun light into electricity by the absorptions of photons and the generation of electron-hole pair which is the main charge carriers for giving electricity. The materials from which the cell is fabricated play a crucial role in the determination of its properties especially the efficiency. Among a lot of materials, semiconductors (SCs) are used in the construction where the gap is a key factor. Germanium and silicon are the most and oldest studied SCs because of their useful in a lot of fields including thin film solar cells, thin film transistors, light emitter devices, photodetectors and synaptic devices as well as nonvolatile memories [1] [2].

The Silicon has a gap of around 1.12 eV at room temperature this allows it to absorb sun light and this material is an active layer in the solar cell. It has different structures crystalline and its opposite amorphous one. But due to the defects and low efficiency plus the diffusion of hydrogen, the mixture of both structures gives another one called microcrystalline (mc-Si :H) and nanocrystalline silicon that was discovered by Veprek and Marecek in 1968. During the last few years, the researchers have extensively studied on the hydrogenated nanocrystalline silicon (nc-Si :H) thin films for different energy applications since the early 1990s.

nc-Si :H and μc-Si :H exhibit superior doping efficiency, higher mobility, low absorption with those of hydrogenated amorphous silicon thin films [3]and high stability under illumination as well as higher conductivity [4]. A variety of growth techniques have been used to prepare this type of silicon. These techniques include plasma enhanced chemical vapor deposition PECVD [5]. An impurity such as boron significantly influences the crystallinity [6] and low-temperature desposition is needed for better crystallinity [7].

The properties of nc-Si :H material are still not well understood due to its structure complexity. The conventional structural picture of nc-Si :H materials includes crystalline nanograin with sizes arround 5 to 20 nm [8][9], this nanocrystals form columns with a diameter of (nm) and tend to grow perpendicularly to the film surface, hydrogenated amorphous often called ‘Tissu’ and voids are also found within this material [10][6][11].

The electrical properties of any material are strongly related to the spatial arrangement of atoms and the phases that form the structure. This latter is heterogenous for nc-Si :H material and its complex configurations make very difficult all attempts to correlate the structure properties with electrical transport mechanism [6]. The conduction mechanisms are discussed in diffrent models that involve potentiel barriers at grain boundaries, tunneling, hopping and percolation [12]. Differences and similarities between intrinsic and doped nc-Si:H conductivity were observed and these are also explained on the basis of recently published studies [13].

For a better understanding of the physical origins of conduction behaviors in the nc-Si :H, it involves to take into consideration the possible conduction mechanisms between two phases : two crystallites in large grain (column), between large crystalline grains (potentiel barrier between them) and between crystalline/amorphous which depicts the potentiel barrier of the heterojunction [14]. The main problem regarding such composites is then the determination of the dominant electrical conducting network and the related transport mechanism as descibed for microcrystalline silicon by [15]. For this propose, We attract a considerable attention on the simulation study of nanocrystalline silicon based on simulation model described in previous published works [16] [17] , as well as the seto's model which is well described in [18]. The conduction mechanisms occurring in these cells will be done with a developed version of AMPS program so called wxAMPS [19].

Plus this general introduction, the present manuscript contains two chapters where in the first one we discussed the solar cell and the importance of silicon in its different structures and the possible models of transport mechanism. The second chapter is for the simulation procedures and the results which were compared to experimental ones. At the end we conclude this document by a general conclusion and perspectives in which we highlight the most important efforts and the good results indicated in this work.

Références

[1] D. Shan, Y. Cao, R. Yang, H. Wang, et T. Tao, « The Carrier Transport Properties of B-Doped Si Nanocrystal Films with Various Doping Concentrations », *J. Nanomater.*, vol. 2020, p. 1-7, août 2020, doi: 10.1155/2020/3698543.

[2] D. Shan, M. Qian, Y. Ji, X. Jiang, J. Xu, et K. Chen, « The Change of Electronic Transport Behaviors by P and B Doping in Nano-Crystalline Silicon Films with Very High Conductivities », *Nanomaterials*, vol. 6, nº 12, p. 233, déc. 2016, doi: 10.3390/nano6120233.

[3] H. N. Liu, Y. L. He, F. Wang, et S. Grebner, « Effect of grain boundary states on CPM spectra of hydrogenated nanocrystalline silicon », *J. Non-Cryst. Solids*, vol. 164-166, p. 1005-1008, déc. 1993, doi: 10.1016/0022-3093(93)91168-3.

[4] R. K. Tripathi, O. S. Panwar, I. Rawal, B. P. Singh, et B. C. Yadav, « Study on nanocrystalline silicon thin films grown by the filtered cathodic vacuum arc technique using boron doped solid silicon for fast photo detectors », *J. Taiwan Inst. Chem. Eng.*, vol. 86, p. 185-191, mai 2018, doi: 10.1016/j.jtice.2018.01.051.

[5] W. Wei, G. Xu, T. Wang, et W. Z. Shen, « Carrier conduction in heterojunction of hydrogenated nanocrystalline silicon with crystal silicon », *Thin Solid Films*, vol. 515, nº 7-8, p. 3997-4003, févr. 2007, doi: 10.1016/j.tsf.2006.09.052.

[6] D. Benlakehal, A. Belfedal, Y. Bouizem, J. D. Sib, L. Chahed, et K. Zellama, « Electronic transport mechanism in intrinsic and doped nanocrystalline silicon films deposited by RF-magnetron sputtering at low temperature », *Superlattices Microstruct.*, vol. 100, p. 228-236, déc. 2016, doi: 10.1016/j.spmi.2016.09.035.

[7] Y. Hamakawa, *Thin-Film Solar Cells: Next Generation Photovoltaics and Its Applications*. Berlin, Heidelberg: Springer Berlin Heidelberg, 2004.

[8] S. El Whibi *et al.*, « Optimized nc-Si:H thin films with enhanced optoelectronic properties prepared by micro-waves PECVD used as an effective silicon surface passivation layer », *J. Mater. Sci. Mater. Electron.*, vol. 30, nº 3, p. 2351-2359, févr. 2019, doi: 10.1007/s10854-018-0508-9.

[9] J. J. Lu, J. Chen, Y. L. He, et W. Z. Shen, « Band offsets and transport mechanisms of hydrogenated nanocrystalline silicon/crystalline silicon heterojunction diode: Key properties for device applications », *J. Appl. Phys.*, vol. 102, nº 6, p. 063701, sept. 2007, doi: 10.1063/1.2779267.

[10] D. Cavalcoli, F. Detto, M. Rossi, A. Tomasi, et A. Cavallini, « The electrical conductivity of hydrogenated nanocrystalline silicon investigated at the nanoscale », *Nanotechnology*, vol. 21, n° 4, p. 045702, janv. 2010, doi: 10.1088/0957-4484/21/4/045702.

[11] B. Yan *et al.*, « On the bandgap of hydrogenated nanocrystalline silicon thin films », in *2010 35th IEEE Photovoltaic Specialists Conference*, Honolulu, HI, USA: IEEE, juin 2010, p. 003755-003760. doi: 10.1109/PVSC.2010.5616075.

[12] W. Fuhs, « Recombination and transport through localized states in hydrogenated amorphous and microcrystalline silicon », *J. Non-Cryst. Solids*, vol. 354, n° 19-25, p. 2067-2078, mai 2008, doi: 10.1016/j.jnoncrysol.2007.09.008.

[13] C. Patra et D. Das, « Intrinsic, P-doped and B-doped nanocrystalline silicon thin films grown at room temperature on flexible substrates for photovoltaic applications », *Mater. Today Proc.*, vol. 62, p. 5110-5113, 2022, doi: 10.1016/j.matpr.2022.02.456.

[14] P. Abboud, F. Martinez, R. Amrani, D. Habib, S. Parola, et Y. Cuminal, « Characterization and modeling of electrical transport in undoped hydrogenated microcrystalline silicon », *J. Non-Cryst. Solids*, vol. 477, p. 42-49, déc. 2017, doi: 10.1016/j.jnoncrysol.2017.09.045.

[15] I. Balberg, Y. Dover, R. Naides, J. P. Conde, et V. Chu, « State distribution in hydrogenated microcrystalline silicon », *Phys. Rev. B*, vol. 69, n° 3, p. 035203, janv. 2004, doi: 10.1103/PhysRevB.69.035203.

[16] M. Chahi, A. Bouhekka, J. D. Sib, A. Kebab, Y. Bouizem, et L. Chahed, « Optoelectronic properties simulation of hydrogenated microcrystalline silicon Schottky diode », *Phys. Status Solidi C*, vol. 7, n° 3-4, p. 640-645, avr. 2010, doi: 10.1002/pssc.200982691.

[17] S. Tripathi, N. Venkataramani, R. O. Dusane, et B. Schroeder, « One-dimensional simulation study of microcrystalline silicon thin films for solar cell and thin film transistor applications using AMPS-1D », *Thin Solid Films*, vol. 501, n° 1-2, p. 295-298, avr. 2006, doi: 10.1016/j.tsf.2005.07.199.

[18] G. Y. Hu, R. F. O'Connell, Y. L. He, et M. B. Yu, « Electronic conductivity of hydrogenated nanocrystalline silicon films », *J. Appl. Phys.*, vol. 78, n° 6, p. 3945-3948, sept. 1995, doi: 10.1063/1.359914.

[19] Y. Liu, D. Heinzel, et A. Rockett, « A revised version of the AMPS simulation code », in *2010 35th IEEE Photovoltaic Specialists Conference*, Honolulu, HI, USA: IEEE, juin 2010, p. 001943-001947. doi: 10.1109/PVSC.2010.5616225.

CHAPTER 1

GENERALITIES ABOUT SILICON

1. Introduction

Among a lot of materials, semiconductors are very important in technology due to their useful. Germanium and silicon are the most and oldest known semiconductors where the first has a small gap about 0,7 eV the seconds gap is 1,12 eV at room temperature [1]. These materials are used in several fields especially in solar cells which is the main road of our future and contents with areas that have sun light can take benefit from their positions on the ground. North Africa countries including Algeria have the sun light in desert and we can do a lot of in this domain. We do believe that one of the most important topics of research in Algeria should be the photovoltaic that can help us in preserving our fossil energy like natural gas and petrol. Another thing that encourages us to think about this is the huge surface of Algeria (2 381 741 km^2) compared to the population which is less than 45 million. In the desert the distance between cities and villages in some cases is very long which make the connection by electricity very expensive and takes time. These factors prove the necessity for solar cells in our society.

2. The need for solar energy (photovoltaic PV)

Solar cells can produce power; however semiconductors (SCs) are needed for this generation. The SCs materials combine the properties of metals (no band gap) and insulators (large band gap) [2], in fact, the sun provides a vast amount of energy: according to Markvart (2000), the solar power received on Earth's surface during one hour is equivalent to the needs of the entire human population for an entire year. When the sun light turns directly into electricity, it produces us photovoltaic power (PV) [3] .where the gap of the material is a crucial factor in this phenomenon. Silicon is one of the SCs that satisfies this condition due to its gap of 1,12 eV which allows it to absorb coming light. The cell cannot be used alone but linked to others to form a module then panel and finally array, as shown in figure 1, that we use to provide electricity for building and heating.

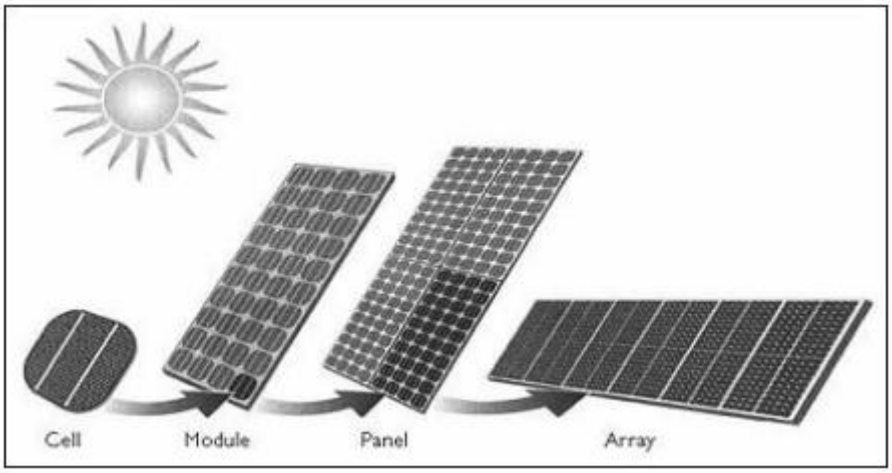

Figure 1. The Relationship among cell, module and array [4].

After a long time of shining and using, light-induced degradation effect is known as the "Staebler-Wronski" effect [5]. This effect is strongly linked to the structure of silicon and changes it negatively by reducing the efficiency of the cell. This latter contains many layers as illustrated in the figure 2 here bellow. As this scheme indicates, the important layer is the active one usually made of silicon that can absorb light and turn it to the creation of electron-hole pair which is the sources of electricity that we need in our daily life. The first layer is for protection and the last one plays the role of reflector of light to increase its probability of absorption when returning back to the bulk of the cell having multi-reflection paths.

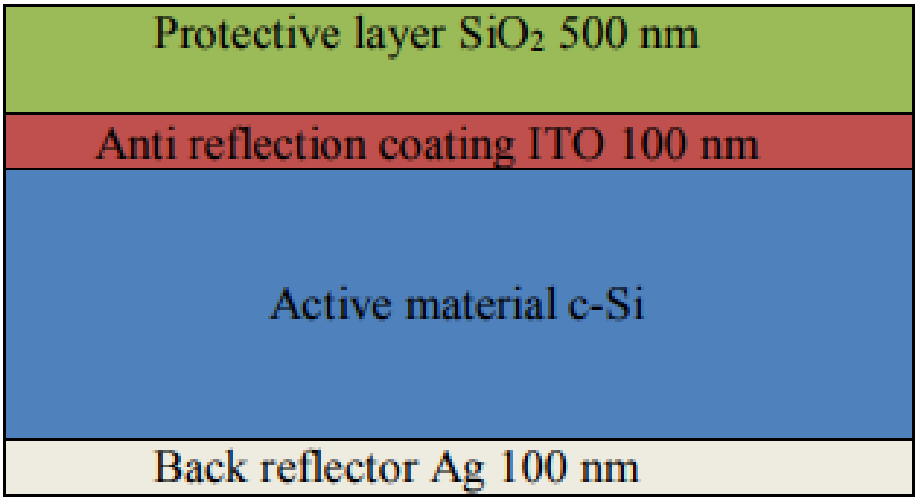

Figure 2. The structure of solar cell [2]

The material from which the active layer is made, usually silicon, has a great importance and researchers focus on it to develop and master its properties.

2.1. The role of silicon thin films in PV

The crystalline silicon (c-Si) and poly- (or "multi-") crystalline silicon (poly-Si) technology continues to have a significant amount of market share these years we live in. However, amorphous silicon (a-Si:H) thin films in particular are becoming more and more alluring. For small-size applications like solar calculators, a-Si:H solar cells have been introduced for quite some time. However, large a-Si:H solar modules also have a number of appealing advantages over "traditional" silicon wafer-based modules. The major one is arguably their significant medium-term potential for cost reduction. Only a very thin layer of silicon (about one millimeter thick) is employed in silicon thin-film technology. Glass is often the substrate on which the active layers are placed; however alternative substrates like stainless steel are also possible. The photovoltaics generate only a limited amount of energy; for this reason many cells are connected to each other to create a solar panel. Silicon is very important in solar cell and it exists in nature under different structure as it will be discussed here bellow.

3. Different structures of silicon

3.1. Crystalline silicon c-Si

The atomic composition of crystalline silicon c-Si is the atomic arrangement of crystalline semiconductors means that it is almost free from defects. c-Si periodicity results in an empty forbidden energy band where there is no intermediate state between the valence band (BV)and the conduction band (BC). The charge carrier (electrons and holes) will be able to move effortlessly due to this periodicity, with mobility [6]

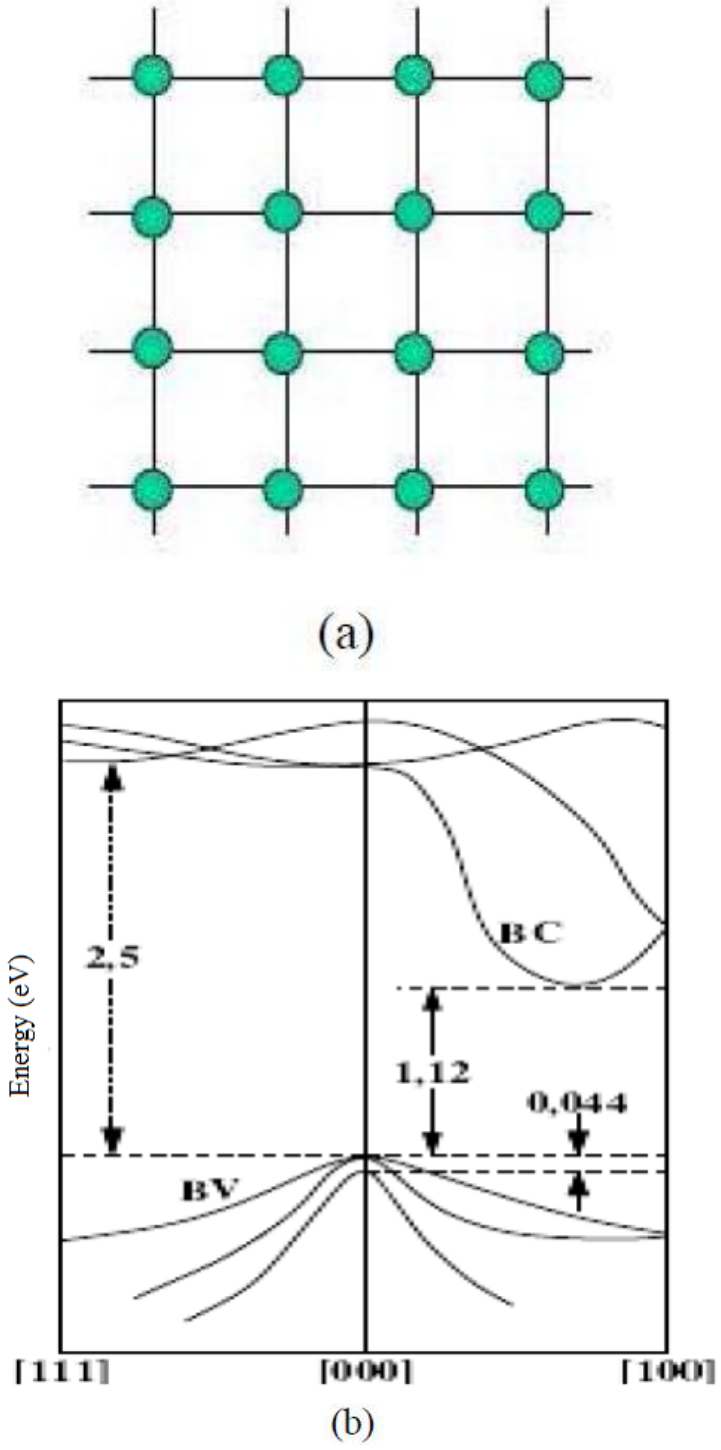

Figure 3. Schematic structure diagrams of a) crystalline silicon network and b) corresponding energy bands [7]**.**

3.2. Hydrogenated amorphous silicon a-Si:H

The a-Si:H material exhibits no long-range order in contrast to the rigid periodic atomic structure found in crystalline silicon. Since there is no long-range organization, the material has peculiar properties such band tail states and dangling bonds. The absence of a long-range system is one of the obvious differences, the difference is due to many disruptions.

In these materials the chemical bonding of atoms is a random covalent network; the disorder variation in the angles between bonds eliminates the regular lattice structure of its crystalline counterpart. Amorphous silicon gap is around of 1.7 Ev. The Dangling connections act as reconfiguration hotspots and significantly shorten the carrier's life. Worse, the defects suspend Fermi's energy level, preventing the use of P- or n-type steroids for amorphous silicon [8]. Numerous methods have been used to deposit amorphous silicon. Among these, PECVD was the first to generate high-quality, photosensitive a-Si:H thin films. The most popular method for depositing a-Si:H in use today is PECVD. The main disadvantage of a-Si:H is that with prolonged sun light exposure, the material quality and solar cell performance degrade [9]. Conduction and valence band tails in this material extend to the middle of the prohibited band due to structural instability

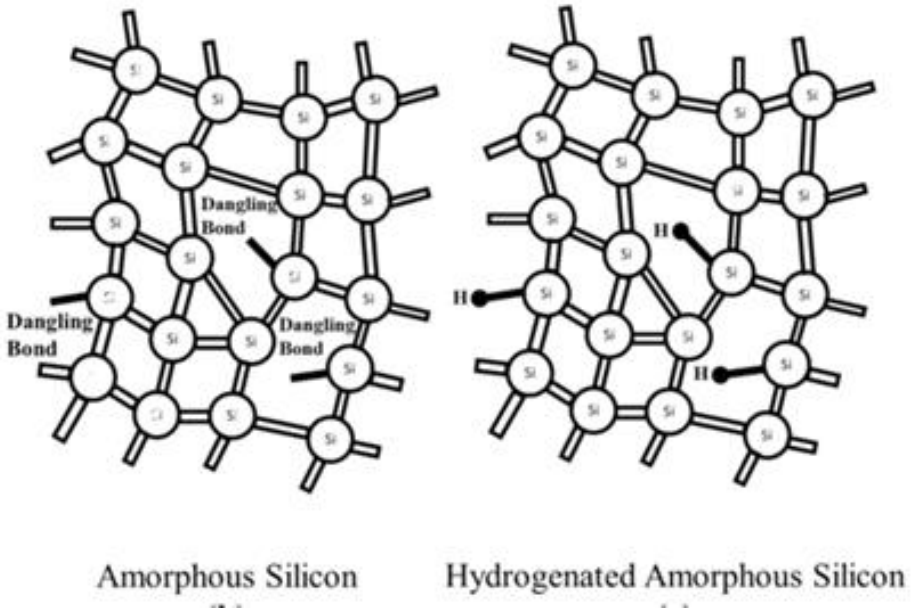

Figure 4. Schematic structure diagrams of amorphous silicon, and hydrogenated [10]

The corresponding diagram structure of amorphous and hydrogenated amorphous silicon is given here bellow.

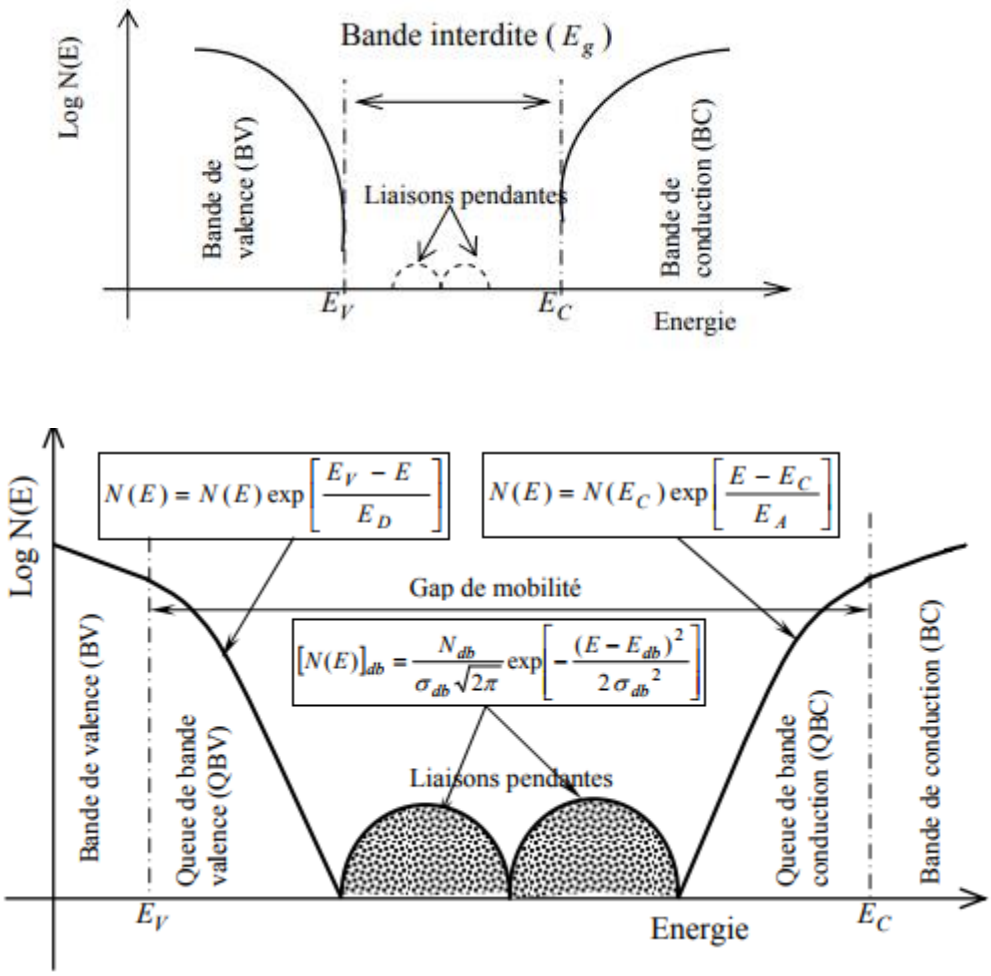

Figure 5. Density of States DOS of a- crystalline, b-amorphous and hydrogenated amorphous silicon [6].

From this figure it is very clear that gap of crystalline silicon has no defects state only if it is doped. However, the continuous of states in the gap for amorphous and hydrogenated amorphous silicon is due defects in the structure. Hydrogen atoms are small and have only one electron which gives them the possibility to penetrate in the amorphous structure making covalent bonds and therefore they strongly reduce the dangling bonds in the amorphous material. For this reason the density of states in the gap is reduced to bellow than 10^{17} cm^{-3} compared to the first one 10^{19} cm^{-3}.

3.3. Polycrystalline silicon poly-Si

Due to the high price of fabricating crystalline silicon material; researchers created polycrystalline silicon in the 1970, which is nearly identical to microcrystalline (same gap). The polycrystalline structure is more resistant to reverse voltage because the power is

dissipated between the grain boundaries and subsequently across the entire surface, resulting in a conversion ratio that ranges from 11 to 13%. **[5]**[11]

3.4. Microcrystalline silicon µc-Si

A microcrystalline material is defined as a material composed of crystalline of nanometre size (1 to 100 nm) [7]. Crystalline lenses are arranged in columns separated by a zone of disorder (high defect density). As scientists differentiate between µc-Si:H and poly-Si by the manufacturing process[12]**.** The term polycrystalline frequently refers to the material crystallized by laser or thermal annealing, while the term microcrystalline refers to the material produced by plasma [8]. By using high-frequency waves and plasma-powered steam, microstalin is created chemically**.** Compared to single phase materials like a-Si:H and c-Si, µc-Si:H exhibits a significantly more complex transport mechanism. The crystalline volume percentage and transit route affect the electrical characteristics of µc-Si:H. microcrystalline has a gap at around 12 eV **.**

3.5. Nanocrystalline silicon nc-Si:

The silicon nano-crystal consists of a silicon amorphous and crystalline (cones or small grains). The grain size of nc-Si varies from (1to 30 nm). In general, a material composed of a few crystals encased in an amorphous tissue. It's supposed to be a rotating pile of c-Si and a-Si. The band gap of nano-crystalline silicon can vary depending on factors such as the size and shape of the crystallites, the band gap of nano-crystalline silicon can range from about 1.5 eV to 2.5 eV .The temperatures at which crystalline nanosilicon deposits can vary depending on the method used for deposition. Some common methods of deposition include plasma-enhanced chemical steam deposition (PECVD) and chemical steam deposition of hot wire (HWCVD). In PECVD, the temperature usually ranges from 150 to 350 ° C, while in HWCVD, the temperature can be higher, ranging from 500 to 700 ° [8]

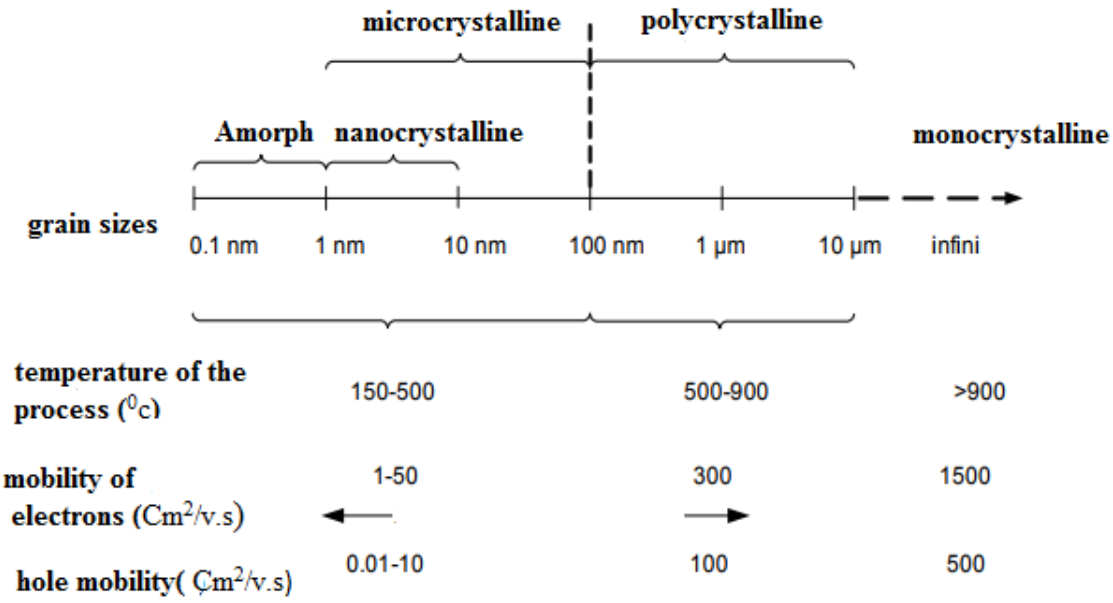

Figure 6. Names of different structure according to the size of crystallites [13]

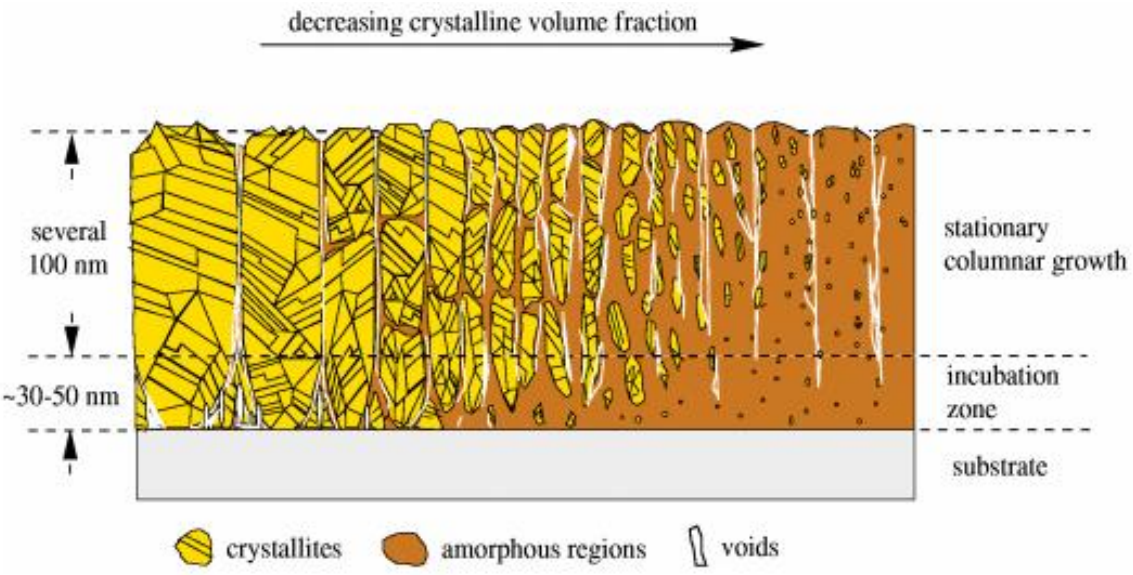

Figure 7. Microcrystalline silicon structure **[8].**

4. Electrical properties of nanocrystalline silicon

Conductivity and mobility are the variables that we utilize to describe the material's electrical properties.

4.1. Current density and conductivity

The current density and conductivity are given by expressions (Eq.1) and (Eq.2) **[14]**respectively**:**

$$J = J_0 \exp(-E_a/k_BT) \qquad \text{(Eq.1)}$$

$$\sigma = \sigma_0 \exp(-E_a/k_BT) \quad \text{(Eq.2)}$$

E_a is the activation energy

j_0 and σ_0 are the pre-exponential factors

k_B Boltzman constant

T the temperature.

The contribution by direct transmission of radiation is negligible (less than 1%) for pure silicon up to 1400'K and is probably negligible at all temperatures up to the melting temperature [15].

The perceived computational power restriction makes it challenging to simulate the heat conductivity in crystalline solids. If it is assumed that the simulation domain must have a mean free path of one, then. To the best of our knowledge, prior publications only offered actual thermal conductivity values in amorphous structures and crystals, which have low thermal conductivity values. However, several previous MD studies on the thermal conductivity are based on non-equilibrium approaches that impose a temperature gradient.

Conductivity increases by several orders of magnitude from the characteristic values of amorphous silicon when the crystalline fraction exceeds 40% [14].

a- The pre-exponential factor of conductivity

It provides details on how the crystalline fraction varies. When one is in a regime of columnar growth [14], this component increases with the crystalline fraction and sharply falls when the joints between the columns appear.

This behavior is explained by the fact that obstacles between columns, rather than the transition between the small crystals, limit transport in microcrystalline silicon in the direction parallel to the substrate.

b- Activation energy

This type of impurity is avoided by using gases reducers such as SiF4 [5] or, as an example, utilizing phosphorous doping as compensation.

Energy for **µ**c-Si activation: typically varies between 0.6 and 0.4 eV. The activation energy of the properly crystallized material is close to 0.5 eV. The substance's activation energy is lower when it is used than it is when it is inactive. The substance may have impurities such integrated oxygen atoms in the layer, however this does not imply that they are contaminated [5].

c- Coplanar and transversal conductivity

If the structure of the considered silicon semiconductor is not homogenous according to the two directions transversal and longitudinal (coplanar) so the conductivity will not be the

same in both directions. For this reason we have to take in consideration the direction where speaking about conductivity. A difference appears also when taking a cross section of the incubation layer between the substrate and the bulk of silicon material which means if one goes a long the incubation layer it is like we have only amorphous structure but for a transversal direction we will have both amorphous and crystalline structures.

4.2. Mobility

The measurement of conductivity by microwave reflection resolved in time, or TRMC, is one method of determining local mobility in precision crystalline silicon [16]. We also mention the DTRMC (diffuse TRMC) method for sporadic mobility [17]. When the crystalline fracture reaches a stable condition, the fundamental motion is saturated [18].

Table1. Magnitude order of mobility of holes and electrons at room temperature

	c-Si		a-Si	
	Electrons	**Holes**	**Electrons**	**holes**
Mobility ($cm^2.v^{-1}.s^{-1}$)	**1350**	**450**	**20**	**2**

We have two types of mobility the one due to the effect of filed and the second one is mobility of carriers. The transport is not the same in both directions transversal and longitudinal due to the following reasons.

- The presence of recombination centres in the grain boundaries and at the surface of microcrystalline silicon [19].
- The presence of amorphous interface between the substrate and the deposited thin film layer. Usually the mobility increases when going far away from this interface [20].

4.3. Transport in μc-Si (nc-Si)

Microcrystalline silicon is a heterogeneous material because of the presentence of two different phases the crystalline and amorphous one and the conductivity is anisotropy due to the colonel structure [21] [13].

4.4. Models of transport of charge

There are a lot of models that explain the transport in nanocrystalline and microcrystalline silicon material. Some of them are derived from the model of Seto. In the following part we are going to describe the modification in Seto model to explain the transport in this complex material.

a- Adapted Seto Model

This model is based on the principle that the structure of microcrystalline material is composed of crystallites separated by grain boundaries and a disorder zone and for this reason we get a difference in the concentration of defects in the crystallites and the grain boundaries. There is a big difference in the application of Seto model on the microcrystalline and poly-crystalline materials because in the pol-crystalline silicon the crystallites are supposed to be perfect however in the micro-crystalline the grain boundaries between columns play a crucial role in the determination of the transport of carriers [22] [23].

b- Homogenous Model

The previous model of Seto was modified to be applied on micro-crystalline and the new name is homogenous model [13]. In this case we consider that the transition between the density of defects between the crystallites and the grain boundaries is not abrupt like indicated in the following figure.

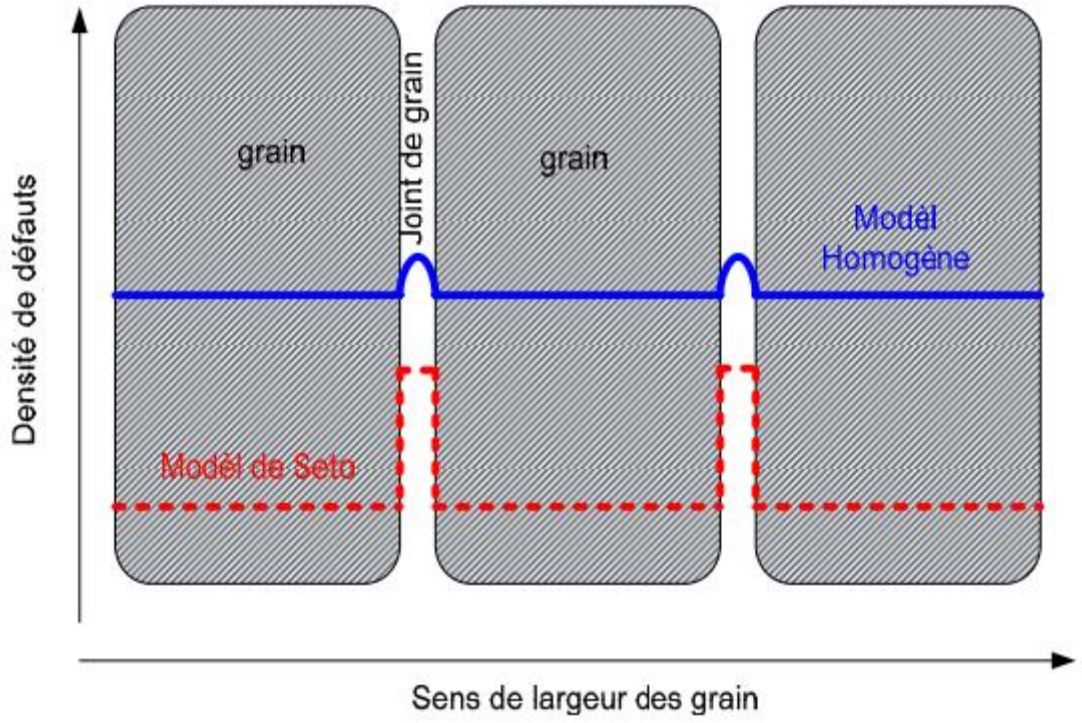

Figure 8. The distribution of defects as indicated by Seto model and homogenous one [13].

There are other models that can be applied to describe the electronic transport but they are applied for materials that have an important amorphous phase like heterojunction model [24]. Where the amorphous phase is important in this case the transport is controlled by it and the mobility of careers holes and electrons is compared to the ones of a-Si:H.

5. Growth model of μc-Si:H (nc-Si)

The figure 8 bellow shows the surface and the model of the growth of microcrystalline and nanocrystalline silicon.

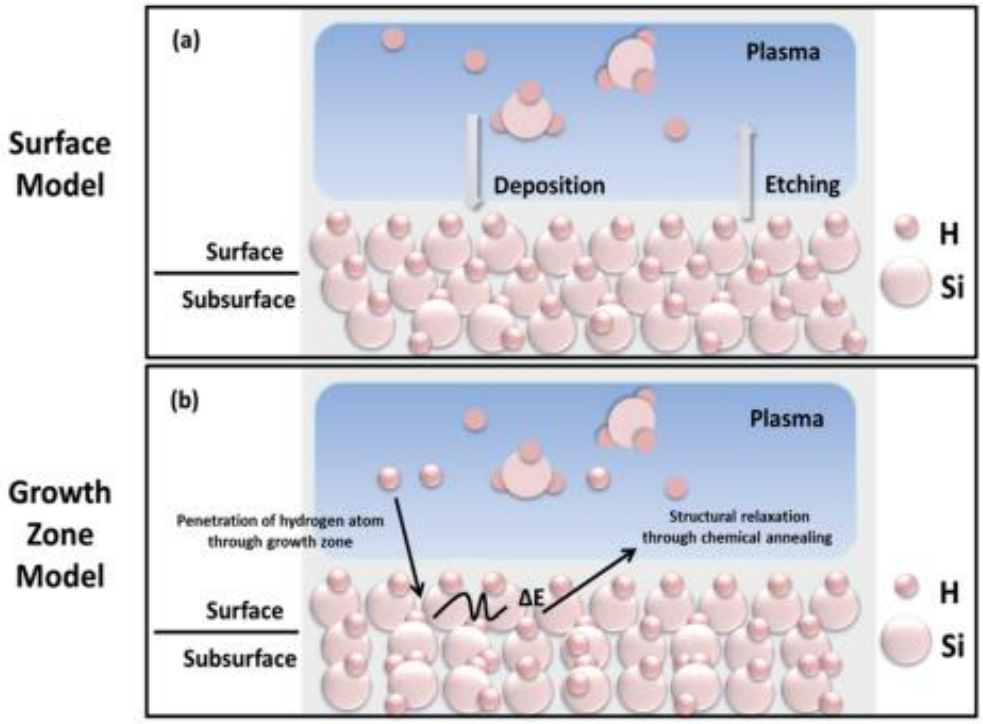

Figure 9. Schematic representation of a- the surface model and b-growth zone model for nc-Si:H [25].

The morphology of microcrystalline material is composed of:

- **Interface layer:** called also memory layer which appears in the beginning of growth and it is the first incubation layer that make the contact between substrate and the other material body. The structure of layer is amorphous due to the conditions of deposition, especially if we consider that the crystallites are made in the plasma region before arriving on the surface [13].
- **Bulk Layer:** tit is the best crystalized layer and it comes directly after the interface layer [13].
- **Sub layer:** Situated after the volume or bulk layer and it is damaged compared to it but still a bit crystalized. It is affected by the ions bombardment and the diffusion of hydrogen [26].
- **Surface roughness:** It is the last layer made when finishing the deposition [13].

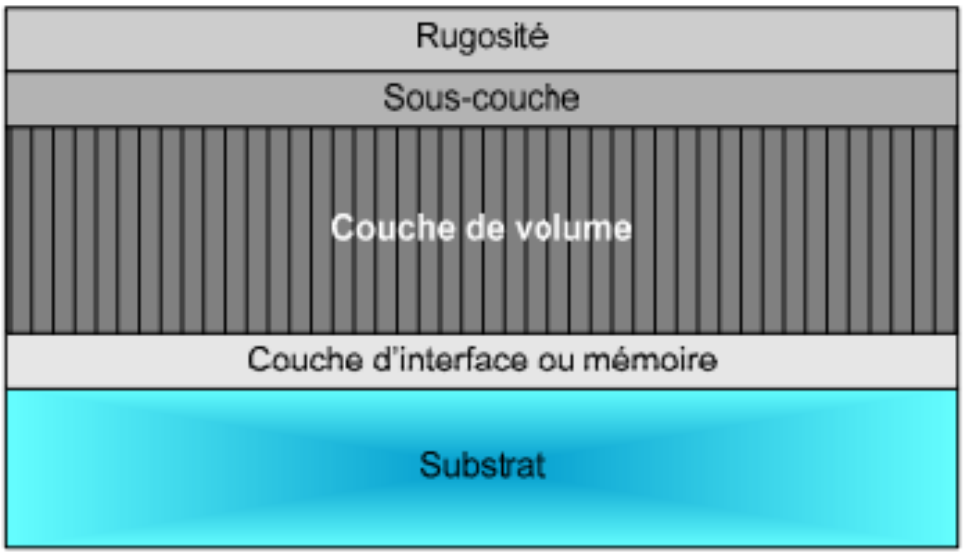

Figure 10. The morphology of microcrystalline silicon [13].

6. Plasma-substrate interactions

The growth of microcrystalline silicon is done by the interaction of plasma components and the surface of substrate where the radicals SiH3 and ions arrived at the surface and contribute in the growth and deposition of μc-Si:H as indicated in the figure 11. Waiting to the formation of crystallites in the plasma other components arrived at the surface which leads to the formation of the first layer of incubation considered as the layer of contact between the bulk and the substrate [13].

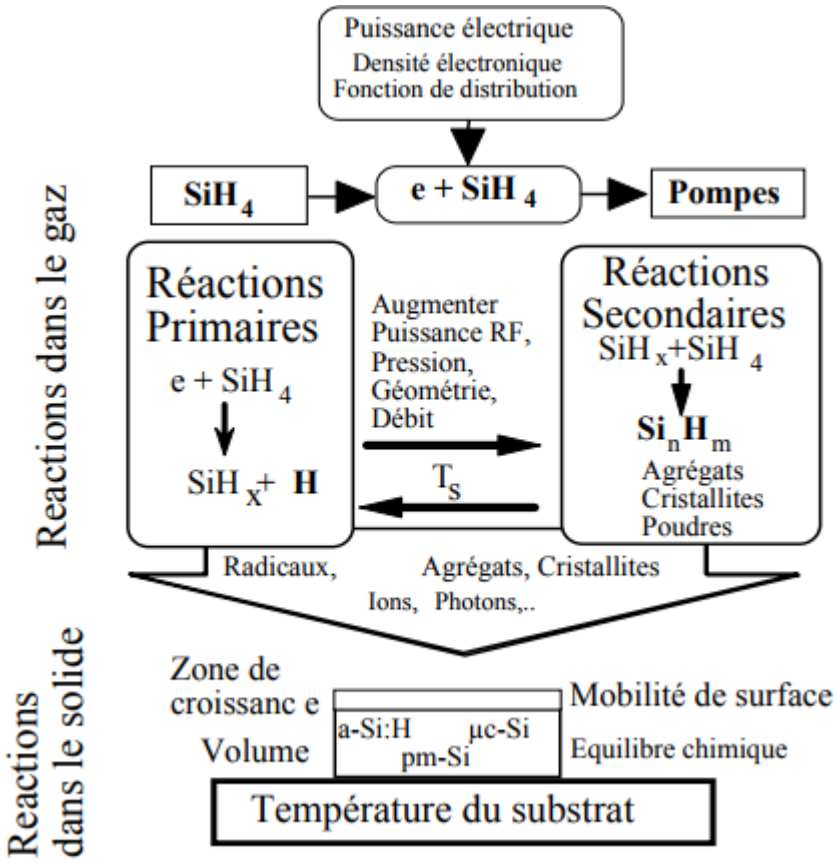

Figure 11. Reactions between plasma and substrate surface [23].

To simulate the electrical properties we need to have an idea about the junctions which are the contact between two different doped SCs. Doping means simply the introduction of exterior atoms or impurities in the SC to get the accepter levels for p doped SC (boron in silicon) and donor levels for n doped Sc (phosphorus in silicon). We have two types of junctions as discussed below.

a-Homojunctions

A typical energy-band diagram for a homojunction is given in Figure. A homojunction consists of a junction between two portions of the same semiconductor, one doped p-type and the other doped n-type, hence the name, *p-n* junction. Typical details of such an energy-band diagram are shown in the figure: the vacuum level E_{vac}, the conduction band edge E_C, the Fermi level E_F , the valence band edge E_V, the band gap E_G , the electron affinity χ_S,and the diffusion potential $q\phi_D$. The work function $q\phi_W$ of a semiconductor is defined as the energy difference $(E_{vac} - E_F)$. Since the work function of the p type portion of the material is greater than that of the n-type portion in figure 12.

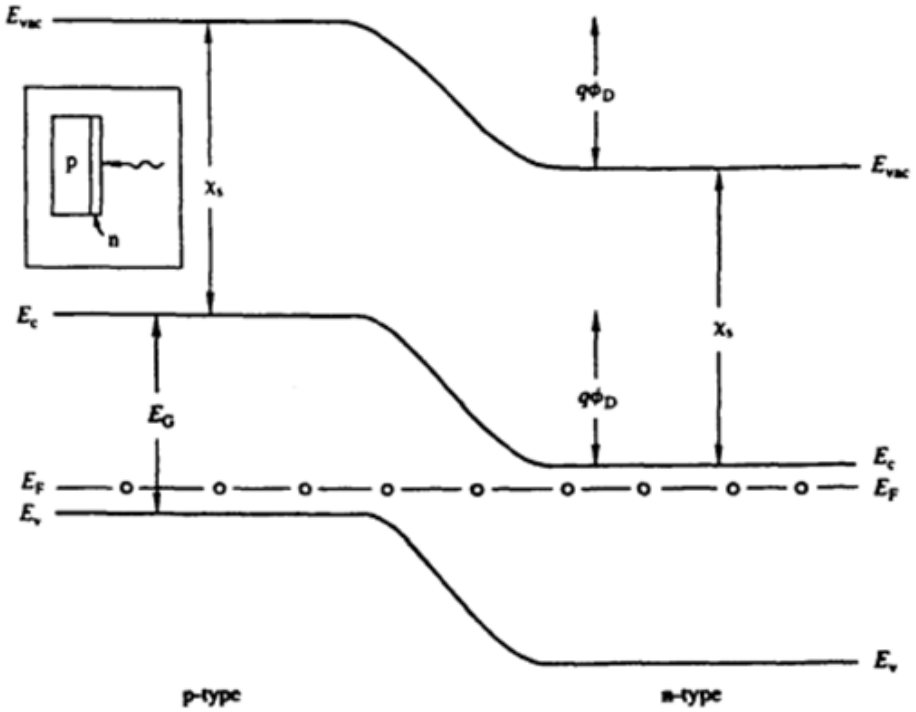

Figure 12. Energy-band diagram for a p-n homojunction with equal densities of doping in the p- and n-type portions

b-Heterojunctions

A p-n heterojunction is a p-n junction formed between two different semiconductors with different band gaps and electron affinities. A typical band diagram for a p-n heterojunction is given in the figure 1.8, where the p-type material is assumed to have a smaller band gap E_{G1} than that of n-type material E_{G2}. the assumption is made that the doping is of the same magnitude for both p and n-type materials, giving equal-width depletion layers on both sides of the junction.

The difference between the electron affinities and band gaps of the two material give rise discontinuities ΔE_C in the conduction band and ΔE_V in the valence band, which can in principle be either positive or negative. Figure 1.8 has been drawn with the desirable assumption that $\chi_1 < \chi_2$, so that an energy spike does not occur in the conduction band impeding electron transport from the ***p*** to the n-type material [27].

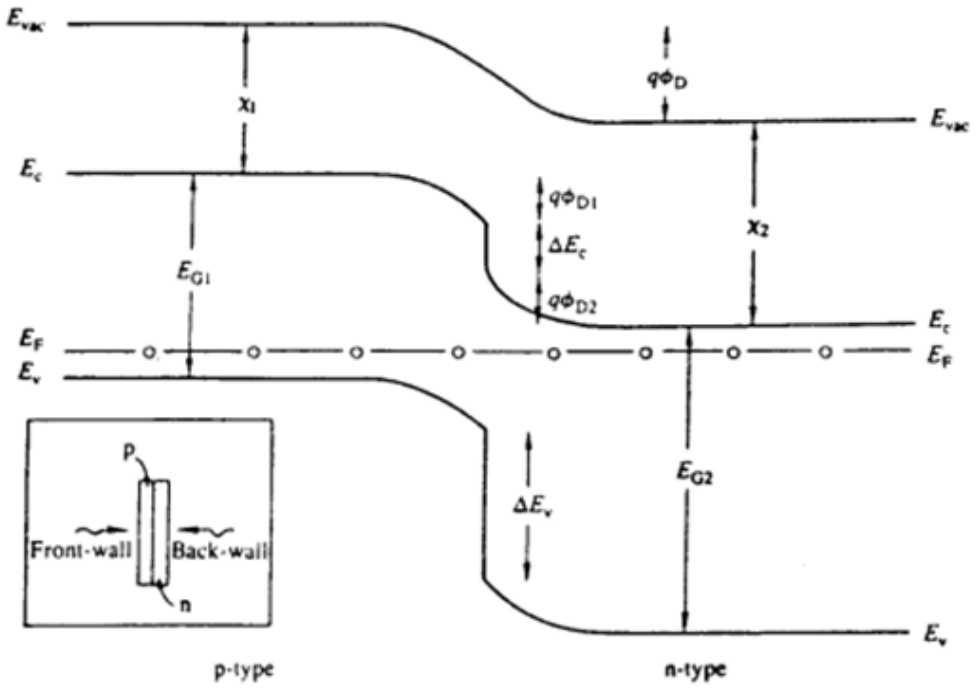

Figure 13. Energy-band diagram for a p-n homojunction with equal densities of doping in the p- and n-type portions, and a choice of material parameters ($\chi_1 < \chi_2$, $E_{G1} < E_{G2}$) such that the are no energy spikes at the junction interface.

7. Conclusion

From this chapter, we conclude that silicon is a very important material for solar cell because it absorbs sun light due its gap of around 1.12 eV. This semiconductor exists on different structure. The well-known and studied is crystalline one and the opposite is the amorphous that contains a lot of defects like distortion in angles and bonds leading to the continuous in the band gap and the dangling bonds of silicon which create deep localized states in the gap. By introducing hydrogen atoms, we can reduce the defects in the gap of amorphous which makes from it a useful semiconductor. But "Staebler-Wronski" effect and the diffusion of hydrogen damage somehow the structure and thus the efficiency is influenced. For this reason the need for best materials is crucial that is why researchers could find poly and micro crystalline silicon as discussed above. These last two semiconductors have a mixture between amorphous and silicon phases which give them different characteristics like good efficiency and a long life time compared to the two first ones (amorphous or crystalline).

REFERENCES

[1] B. I. Shklovskii et A. L. Ėfros, *Electronic properties of doped semiconductors*, Softcover reprint of the original 1st edition 1984. in Springer series in solid-state sciences, no. 45. Berlin Heidelberg: Springer-Verlag Berlin Heidelberg GmbH, 2013.

[2] O. Khiter, « Light trapping by surface texturing in solar cells », Thèse Master, Université Hassiba Benbouali de Chlef, 2020.

[3] C. Droz, « Thin Film Microcrystalline Silicon Layers and Solar Cells: Microstructure and Electrical Performances », Phd thesis, Université de Neuchâtel, 2003.

[4] A. A. T. Alkhalidi et N. H. A. Dulaimi, « Design of an Off-Grid Solar PV System for a Rural Shelter », 2018, doi: 10.13140/RG.2.2.24352.07689.

[5] D. L. Staebler et C. R. Wronski, « Reversible conductivity changes in discharge-produced amorphous Si », *Appl. Phys. Lett.*, vol. 31, nº 4, p. 292-294, août 1977, doi: 10.1063/1.89674.

[6] M. Chahi, « Simulation du fonctionnement des dispositifs électroniques à base de silicium microcristallin µc-Si : H », Thèse de magister, UNIVERSITE D'ORAN ES-SENIA, 2009.

[7] A. Bouhekka, « Faculté des Sciences Exactes et Informatique Département de Physique », Cour Master, Université Hassiba ben Bouali de Chlef, 2018.

[8] R.E.I. Schropp et M. Zeman, *Amorphous and Microcrystalline Silicon Solar cells: Modeling, Materials and Device Technology*. Springer US, 1998. doi: 10.13140/RG.2.1.1429.0001.

[9] Y. Mai, « Microcrystalline silicon layers for thin film solar cells prepared with Hot Wire Chemical Vapour Deposition and Plasma Enhanced Chemical Vapour Deposition », Phd thesis, Institut de recherche en Allemagne.

[10] H. Kang, « Crystalline Silicon vs. Amorphous Silicon: the Significance of Structural Differences in Photovoltaic Applications », *IOP Conf. Ser. Earth Environ. Sci.*, vol. 726, nº 1, p. 012001, avr. 2021, doi: 10.1088/1755-1315/726/1/012001.

[11] A. Pierre, J. M. Lamarche, R. Mercier, et A. Foissy, « Adsorption d'un fluidifiant du ciment sur le carbonate de calcium », *Cem. Concr. Res.*, vol. 19, nº 5, p. 692-702, sept. 1989, doi: 10.1016/0008-8846(89)90040-9.

[12] S. Y. Yoon, S. J. Park, K. H. Kim, J. Jang, et C. O. Kim, « Structural and electrical properties of polycrystalline silicon produced by low-temperature Ni silicide mediated crystallization of the amorphous phase », *J. Appl. Phys.*, vol. 87, nº 1, p. 609-611, janv. 2000, doi: 10.1063/1.371906.

[13] S. Wagner, H. Gleskova, I.-C. Cheng, et M. Wu, « Silicon for thin-film transistors », *Thin Solid Films*, vol. 430, nº 1-2, p. 15-19, avr. 2003, doi: 10.1016/S0040-6090(03)00121-4.

[14] Y. Djeridane, « Synthèse de nanocristaux par plasma froid et leurs rôle dans la croissance de couches minces de silicium microcristallin : Application aux transistors », ÉCOLE POLYTECHNIQUE, 2008.

[15] H. R. Shanks, P. D. Maycock, P. H. Sidles, et G. C. Danielson, « Thermal Conductivity of Silicon from 300 to 1400°K », *Phys. Rev.*, vol. 130, nº 5, p. 1743-1748, juin 1963, doi: 10.1103/PhysRev.130.1743.

[16] J. A. Simmons, S. W. Hwang, D. C. Tsui, H. P. Wei, L. W. Engel, et M. Shayegan, « Resistance fluctuations in the integral- and fractional-quantum-Hall-effect regimes », *Phys. Rev. B*, vol. 44, nº 23, p. 12933-12944, déc. 1991, doi: 10.1103/PhysRevB.44.12933.

[17] S. Kasouit, P. Roca I Cabarrocas, et R. Vanderhaghen, « DTRMC, a probe of transverse transport in microcrystalline silicon », *Thin Solid Films*, vol. 427, nº 1-2, p. 335-339, mars 2003, doi: 10.1016/S0040-6090(02)01204-X.

[18] P. Roca I Cabarrocas, R. Brenot, P. Bulkin, R. Vanderhaghen, B. Drévillon, et I. French, « Stable microcrystalline silicon thin-film transistors produced by the layer-by-layer technique », *J. Appl. Phys.*, vol. 86, nº 12, p. 7079-7082, déc. 1999, doi: 10.1063/1.371795.

[19] T. Unold, R. Brüggemann, J. P. Kleider, et C. Longeaud, « Anisotropy in the transport of microcrystalline silicon », *J. Non-Cryst. Solids*, vol. 266-269, p. 325-330, mai 2000, doi: 10.1016/S0022-3093(99)00719-X.

[20] P. Roca I Cabarrocas *et al.*, « Microcrystalline silicon: An emerging material for stable thin-film transistors », *J. Soc. Inf. Disp.*, vol. 12, nº 1, p. 3, 2004, doi: 10.1889/1.1824232.

[21] B. Rezek, J. Stuchlík, A. Fejfar, et J. Kočka, « Local characterization of electronic transport in microcrystalline silicon thin films with submicron resolution », *Appl. Phys. Lett.*, vol. 74, nº 10, p. 1475-1477, mars 1999, doi: 10.1063/1.123585.

[22] J. Y. W. Seto, « The electrical properties of polycrystalline silicon films », *J. Appl. Phys.*, vol. 46, nº 12, p. 5247-5254, déc. 1975, doi: 10.1063/1.321593.

[23] P. Hapke, U. Backhausen, R. Carius, F. Finger, et S. Ray, « Modulated Hall-Effect Techniques for the Study of Transport Properties of Microcrystalline Silicon with Different Grain Sizes », *MRS Proc.*, vol. 420, p. 789, 1996, doi: 10.1557/PROC-420-789.

[24] J. Kočka *et al.*, « Amorphous/microcrystalline silicon superlattices—the chance to control isotropy and other transport properties », *Appl. Phys. Lett.*, vol. 79, nº 16, p. 2540-2542, oct. 2001, doi: 10.1063/1.1410364.

[25] M. Sharma, J. Panigrahi, et V. K. Komarala, « Nanocrystalline silicon thin film growth and application for silicon heterojunction solar cells: a short review », *Nanoscale Adv.*, vol. 3, nº 12, p. 3373-3383, 2021, doi: 10.1039/D0NA00791A.

[26] B. Kalache, A. I. Kosarev, R. Vanderhaghen, et P. R. I Cabarrocas, « Ion bombardment effects on microcrystalline silicon growth mechanisms and on the film properties », *J. Appl. Phys.*, vol. 93, nº 2, p. 1262-1273, janv. 2003, doi: 10.1063/1.1524707.

[27] R. H. Bube, *Photovoltaic materials*. in Series on properties of semiconductor materials, no. vol. 1. London : River Edge, N.J: Imperial College Press ; Distributed by World Scientific, 1998.

CHAPTER 2

wxAMPS Simulation of Electrical Properties of nc-Si:H:Model and Results

1. Introduction

In this part, the simulated samples were fabricated and studied experimentally by D. Benlakhal et al [1] using radiofrequency magnetron sputtering RFMS technique with RF power 220 W, a gas mixture of 30 % of Ar and 70 % of H_2 and the target – sample holder distance, fixed at 70 mm, were maintained constant for the samples. The deposition rate of 3 and 30 minutes were tested. They investigated the film conductivity via several technological parameters, such as doping type (p and n), deposition rate and crystalline grain size, and comprehensive models current transport. The sizes, shape, and density of crystallites embedded in the amorphous matrix of the all samples were determined by Raman spectroscopy. For the films deposited during 30 minutes and at 100°C, the Raman spectra indicates the important presence of the crystallites in the samples which is described in detail in[1][2].Tables1 and 2in results and discussion section list the experimental findings reported from [1]of all the samples investigated in this study using wxAMPS simulation program.

2. wxAMPS simulation tool

The wxAMPS-1D program is an improved version of AMPS, and was developed by Prof. Angus Rockett and Dr.Yiming Liu at the University of Illinois at Urbana Champaign, in collaboration with Nankai University of China. It is a substantially new solar cell simulator for modelling one dimensional devices composed of various materials. This modified version accepts the same input parameters and ensures the similar physical principles and numerical descriptions of defects and recombination as AMPS [3][4]. In addition, wxAMPS version has the capabilities to include several different tunnelling principles: trap assisted, intra-band, and band-to-band mechanisms [5][6]. It solves simultaneously the Poisson equation and the electron and hole continuity equations using the finite differences method and the Newthon-Raphson technique. wxAMPS is written in C++ and includes a number of revisions to the basic algorithm [4].

The basic equations utilized to determine the performance of the solid state device is Poisson' and the current continuity equations as below.

2.1. Carrier Transport in Semiconductors

The electrical properties of semiconductors are controlled by the concentrations of holes and electrons as well as their ability to flow in a specific direction under the influence of an electric field.

2.1.1.The transport equations:

In order to consider the contribution of both electrons and holes, the total drift (conduction) current is written as:

$$J_{drift} = J_n + J_p = q\mu_n n(x)\vec{E}(x) + q\mu_p p(x)\vec{E}(x) \quad \text{(Eq.1)}$$

Jn and Jp are the electron and hole current densities.

Where n and p are the electron and hole concentrations, μ_n and μ_p are the electron and hole mobilities,and $\vec{E}$ is the electric field.

As with atomic diffusion, the driving force for carrier diffusion is the gradient in electron concentration. For free electrons diffusing along the x – axis, Fick's law applies and it can be written: $\phi_n = -D_n \frac{dn(x)}{dx}$

Where ϕ_n is the flux of electrons (number of electrons per unit area per second) following along the x – axis due to a concentration gradient of electrons. The negative sign in equation indicates that the diffusion occurs in the direction of decreasing electron concentration. For holes, Fick's first law becomes:

$$\phi_p = -D_p \frac{dp(x)}{dx} \quad \text{(Eq.2)}$$

Since the flow of charged particles constitutes an electric current, we can describe diffusion currents due to holes or electrons. These are distinct from drift current:

$$J_{n-dif}(x) = qD_n \frac{dn(x)}{dx} \quad \text{(Eq.3)}$$

$$J_{p-dif}(x) = -qD_p \frac{dp(x)}{dx} \quad \text{(Eq.4)}$$

Where D_n and D_n are the electron and hole diffusion constants.

An interesting situation occurs when both diffusion and drift currents flow. An electric field is present as well as a carrier concentration gradient. The total current densities are written:

$$J_{n-drif-dif}(x) = q\mu_n n(x)\vec{E}(x) + qD_n \frac{dn(x)}{dx} \quad \text{(Eq.5)}$$

$$J_{p-drif-dif}(x) = q\mu_p p(x)\vec{E}(x)) - qD_p \frac{dp(x)}{dx} \quad \text{(Eq.6)}$$

2.1.2. Continuity equations

The continuity equations combine the drift, diffusion, generation and recombination processes into single equation. The continuity equation in one dimension along the x – axis for both electrons and holes can be written as:

$$\frac{\partial n}{\partial t} = \frac{1}{q}\frac{\partial J_n(x)}{\partial x} + \mathcal{G}_n - \mathcal{R}_n \quad \text{(Eq.7)}$$

$$\frac{\partial p}{\partial t} = -\frac{1}{q}\frac{\partial J_p(x)}{\partial x} + \mathcal{G}_p - \mathcal{R}_p \quad \text{(Eq.8)}$$

Where $\mathcal{G}_n$ ($\mathcal{G}_p$) and $\mathcal{R}_n$ ($\mathcal{R}_p$) are the generation and recombination rate of both electron and holes respectively.

2.1.3. Poisson's Equation

Poisson's equation links free carrier populations, trapped charge populations, and ionized dopant populations to the electrostatic field present in a material system. In one-dimensional space, Poisson's equations is given by:

$$\frac{d}{dx}\left(-\varepsilon(x)\frac{dV}{dx}\right) = q[p(x) - n(x) + N_D^+(x) - N_A^-(x) + p_t(x) - n_t(x)] \quad \text{(Eq.9)}$$

Where the electrostatic potential V and the free electron n, free p, trapped electron n_t, and trapped hole p_t, as well as the ionized donor like doping N_D^+ and ionized acceptor like doping N_A^- concentrations are all functions of the position coordinate x. Here, ε is the permittivity and q is the magnitude of the charge of an electron.

In principle, any numerical program capable of solving the basic semiconductor equations could be used for modelling thin film solar cells. The basic equations are the Poisson equation, relating the charge to the electrostatic potential ϕ, and the continuity equations for electrons and holes each of which has two associated boundary conditions. In one dimension, the total cell length is divided into segments by a mesh of grid points, the value of Vi and the electron and hole concentrations ni and pi at each of the segment constitutes the three unknowns states variables of the problem.

In wxAMPS, these three coupled equations, along with the appropriate boundary conditions, are solved simultaneously to obtain a set of three unknown state variables at each point in the device: electrostatic potential, the hole quasi-Fermi level E_{fp}, and the electron quasi-Fermi level E_{fn}. From these three state variables, the carrier concentrations, fields, currents, etc. can then be computed. To determine these state variables, the finite differences and the Newton-Raphson methods are incorporated by the computer. The Newton-Raphson technique iteratively finds the root of a function or roots of a set of functions if given an adequate initial guess for these roots. As noted, once these three state variables are obtained as a function of x, the band edges, electric field, trapped charge, carrier populations, current densities, recombination profiles, and any other transport information may be obtained [7][8].

3. Simulation model

Structurally, The nc-Si: H material is composed of crystalline silicon grains separated by amorphous silicon grains boundaries (GBs). Conduction through the nc-Si film is strongly affected by potential barriers at the GBs, associated with the large density of trapping states caused by defects at the GBs [9].

The experimental study of the optical and electrical properties of the resulting solar cell based on nanocrystalline silicon is complex due to its structure. For further optimization of the solar cell performance, a good understanding of the contribution of each layer and interface (film-substrate) is imperative. These contributions can be investigated by Numerical simulation in order to complement the limitations of experimental work.

In a real polycrystalline material, the crystallites have an unequally distributed size, irregular shapes and orientations [10]. It is composed of small crystallites of size about 30 nm linked together by a few disordered atomic layers, that results in carrier trapping at the grain boundary GBs, creating a potential barrier [11]. The adopted model used to explain the conductive properties of polycrystalline material, originally proposed by Seto, is called the grain boundary trapping (GBT) model [12][13]. It considers a one-dimensional of chain of identical nc-Si having a grain size L, where the GB thickness is small relative to the grain size L. The scheme of a simple picture of the cells modeled in the present simulation is illustrated in Figure 1.In this work, we have applied directly the GBT model for nc-Si :H films which identifies the conduction of nc-Si :H as a thermionic emission and thermal-assisted tunneling processes.

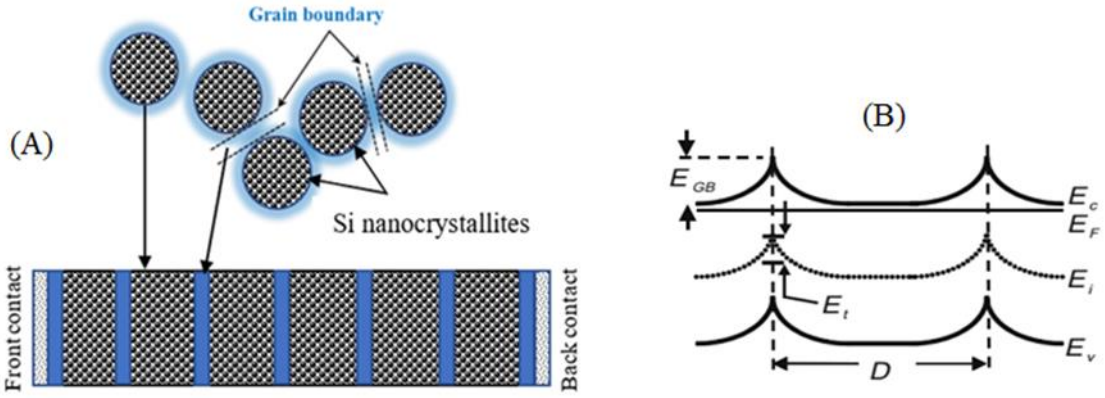

Figure 1. Schematic model simulation: (A) nc-Si constituted by crystalline region (nanocrystallites) and amorphous region (grain boundaries). (B) Simulation modelfollowing the Seto and Le Comber models.

According to the GBT model, we assumed in the first approximation as an alternating stack of a-Si:H (GBs) and c-Si (crystalline grains). This model can be supported by the crystalline and amorphous regions visited by the electrons form one electron to other. In fact, the growth of the material is perpendicular to the substrate and the displacement of the charge carriers can be in transversal or longitudinal directions according to the electrodes disposition [14]. In both cases the simulation model of electron transport is the same. The number of alternatives successive layers, composed the sample, is fixed and the size of the nano-crystallites is assumed to have the same value and varies between 5 nm to 20 nm depending on their volume fraction in the sample.

We have changed the volume crystalline fraction by varying thickness of crystalline silicon layers to examine its influence on the electrical, structural properties and conduction mechanism. In order to compare the experimental findings with those simulated, we must take into consideration the crystalline volume fraction measured by Raman and ellipsometry spectroscopic methods. In our study, the crystalline fraction (X_c) will be calculated by the following formula:

$$X_c = \frac{\sum crystallinelayerthickness}{\sum crystallinelayerthickness + \sum amorphouslayerthickness} \quad \text{(Eq.10)}$$

Three categories (intrinsic, n doped and p doped), with their corresponding X_c, of samples were prepared at T = 100°C and times of 3min and 30 min as indicated below:

- Intrinsic films: I03MIN100 ($X_c = 0$) and I30MIN100 ($X_c = 74\%$)
- N doped films: N03MIN100 ($X_c = 35\%$) and N30MIN100 ($X_c = 72\%$)
- P doped films: P03MIN100 ($X_c = 38\%$) and P30MIN100 ($X_c = 73{,}5\%$)

3.1. Simulation Parameters

The parameters of both c-Si and a-Si layers are summarized in the following figures.

a) Electrical parameters

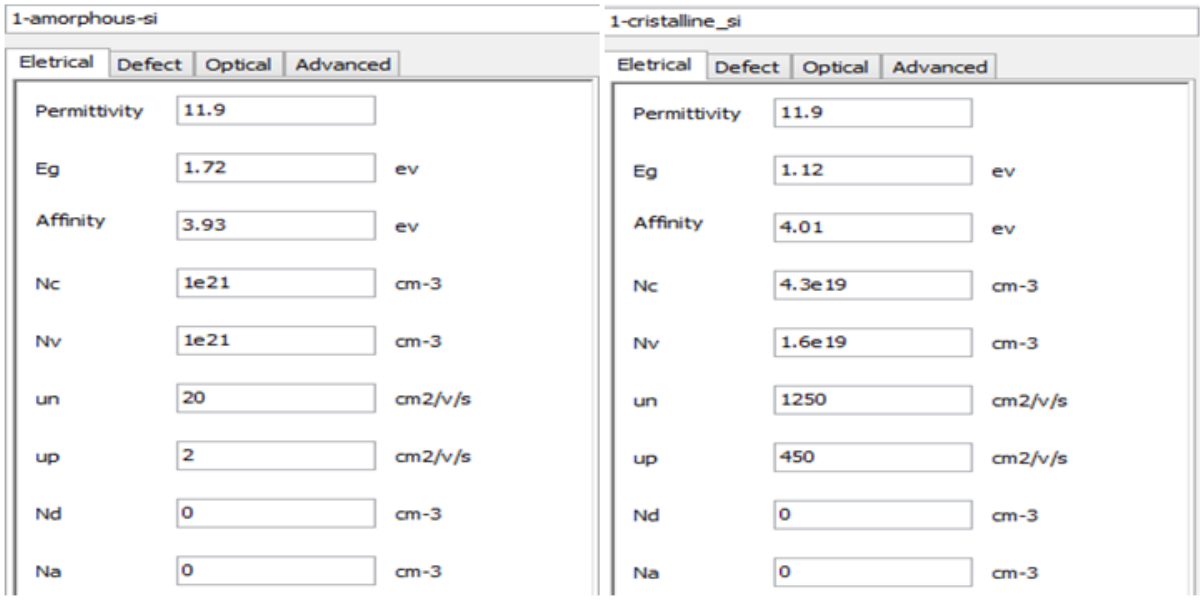

b)Defect parameters (Middle gap)

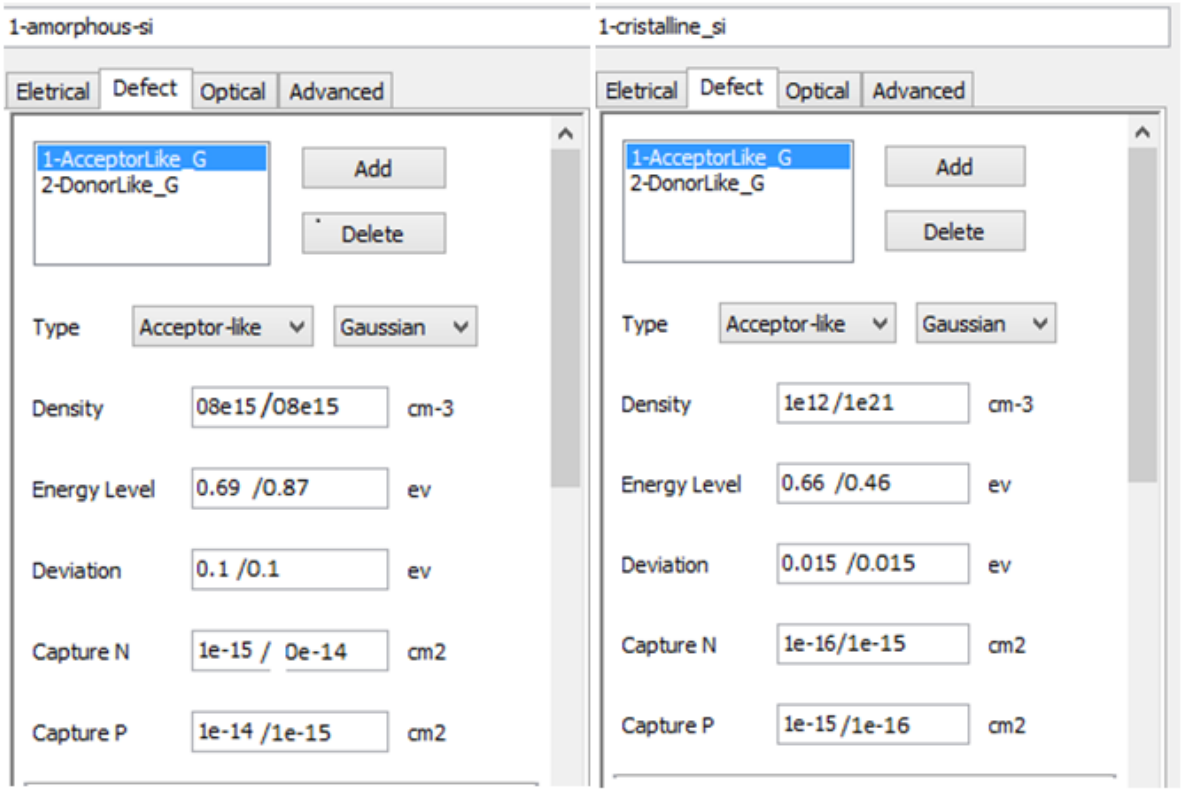

c) Defect parameters (Band tails)

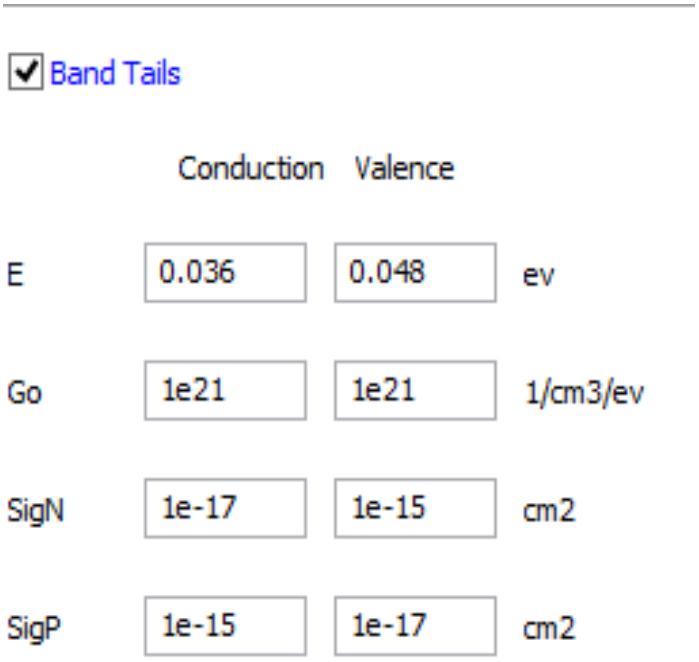

d)Boundary Conditions

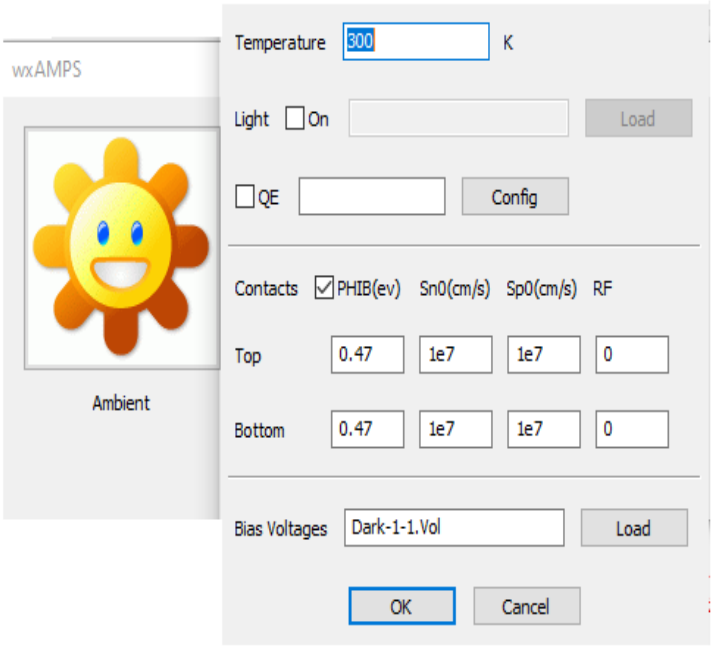

PHIB: represents the height barrier in the contact between the metal and semiconductor

PHIB= $\phi_M - \chi_S$, where ϕ_M is the work function of the metal and χ_S is the electronic affinity of semiconductor(eV).

SN: Surface recombination speeds of electrons (cm/s).

SP: Surface recombination speeds of holes (cm/s).

Bias volatge: Applied voltage on our samples.

4. Results and discussion

The crucial point in modelling a device based on nc-Si:H material is to define the role played by the boundary regions between the crystalline grains and the amorphous matrix. In this transition regions it is supposed to be localized a high concentration of defects in the lattice structure. If the distance between two adjacent grans is enough large this region could be treated similarly to heterojunction. To distinguish one transport mechanism from the others, we employ the well-known general junction rectification model [15] to clarify the relation between the current and the applied forward voltage.

We have to devise different mathematical models which are able to describe the important physical phenomena for a particular situation or for particular device. Moreover, since in some cases we are not interested in all the available physical information, we need simple models which help to reduce the computation cost in the numerical simulations [16].

Based on the approach consideration of nc-Si:H cells as a diode [17], the dark J–V characteristics can be given by the follow formula:

$$J = J_0 \left[exp\ \left(\frac{qV}{nkT} \right) - 1 \right] \quad \text{(Eq.11)}$$

Where k is the Boltzmann constant and n is the ideality factor.

J_0 is the saturation current density. In this case, a very good phenomenological approximation for most diode and solar cells even though the complicated recombination is given by the following relation[18][17] :

$$J_0 \propto exp\left(-\frac{E_a}{kT} \right) \quad \text{(Eq.12)}$$

whereE_a is the activation energy.

It is observed that the nc-Si:H is biphasic material consisting the crystalline and amorphous silicon. Accurate modelling and simulation of thin film solar cells based on nc-Si:H requires models that describe the specific material parameters based on their component such as the amorphous and crystalline phases.

In crystalline semiconductor, carrier transport takes place in extended states inside the energy bands and the high carrier mobilities are limited by scattering at phonons or impurities. The gap states appear as isolated states and electronically communicate with the energy bands only. In our numerical simulation, the atoms of crystalline silicon is well organized which is reflected by absence of band tail in the gap but there is no perfect crystalline structure and the existence of some vacuum create localized states in the middle of the gap. Therefore the density of state (DOS) of crystalline silicon can be parameterized with a donor and an acceptor Gaussian distribution located at midgap with very low value[19][20]. In an

amorphous semiconductor disorder causes localization at the band edges and tails of localized states extend deep into the energy gap. The localized and extended states are separated by mobility edges which for the transport mechanism at higher temperatures play a role quite similar to the band edges in crystalline semiconductors[19].

4.1. Diagram band structure

Figure 2 illustrates the band structure of nanocrystalline silicon samples in thermodynamic equilibrium and non-equilibrium. The magnitudes of the valence and conduction band offsets should up to the difference in band gaps between the materials. We have applied the heterojunction model on our samples as discussed in the chapter I. The difference in bonding between c-Si and a-Si has an effect on the positions of the valence and conduction bands as well, of course but that effect is included entirely in the bulk calculations [21]. If we assume the heterojunction model, we obtained a valence band offset of $\Delta E_V = 0.68$ eV, and the conduction band offset of $\Delta E_C = 0.08$ eV.

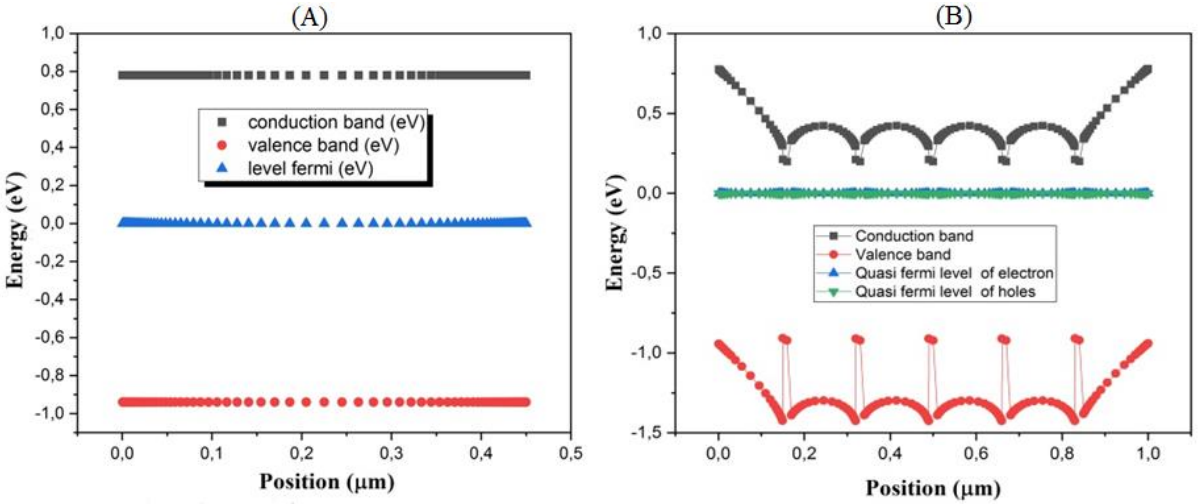

Figure 2. Band diagram of nano-crystalline silicon (A) in thermodynamic equilibrium and (B) in non thermodynamic equilibrium.

4.1.1. Transport mechanisms

Transport mechanisms inside such devices are still not fully understood yet,the one key study of the amorphous crystalline interface provides more information about the electronic transport properties of nanocrystalline silicon. This work focuses on the current voltage (J-V) characteristics method through the interfaces to examine activation energy in nanocrystalline silicon samples under dark condition.

4.1.2. Current-voltage characteristicJVT

The Figure 3 shows the temperature current voltage (JVT) in forward bias voltage. Under dark conditions, the JVT of the solar cell is very similar to that of a diode. A simple diode characteristic is modeling using the equation (Eq.11).

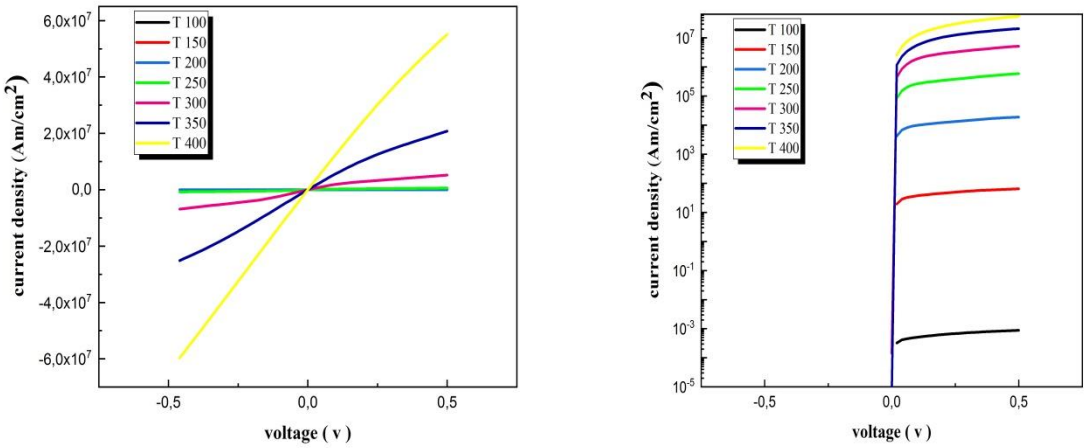

Figure 3. Current density voltage characteristics of nanocrystalline silicon under dark conditions at different temperature values (*Ln(J) vs V)* indicated in right Figure).

Parameter extraction is a fundamental process to evaluate the performance of photovoltaic (PV) devices. The obtained parameters can be used not only to predict the behavior of solar cells but also to obtain essential information about device performance and efficiency [22].

One of these parameters is the pre-exponential J_0(Eq.11), in fitting the dark JVT characteristics, the J_0 factors of the samples in the model is deduced from the slope and y-intercept of the linear regression plot of the equation (Eq.12). The simulated parameter was extracted from generated dark JV data at different temperatures as indicated in the Figure3.

One of the most important parameters that we are looking for is the activation energy which strongly affected by the structure and the type of the considered material as indicated in the following part.

4.1.2.1. Activation energy conductivity

The activation energy in the former case represents the energy difference between the mobility edge and Fermi level, $E_C - E_f$ or $E_f - E_V$. In the latter case, it represents the sum of the energy separation between occupied localized states and the Fermi level, and the mobility activation energy for the hopping process between the localized states[23].

To determine this parameter, we followed a procedure for the entire sample studied in this work. Figure4 represents each intercept with the ordinate axis as function of 1/KT, and the slop of the linear fitting indicates the activation energy as illustrated in bellow.

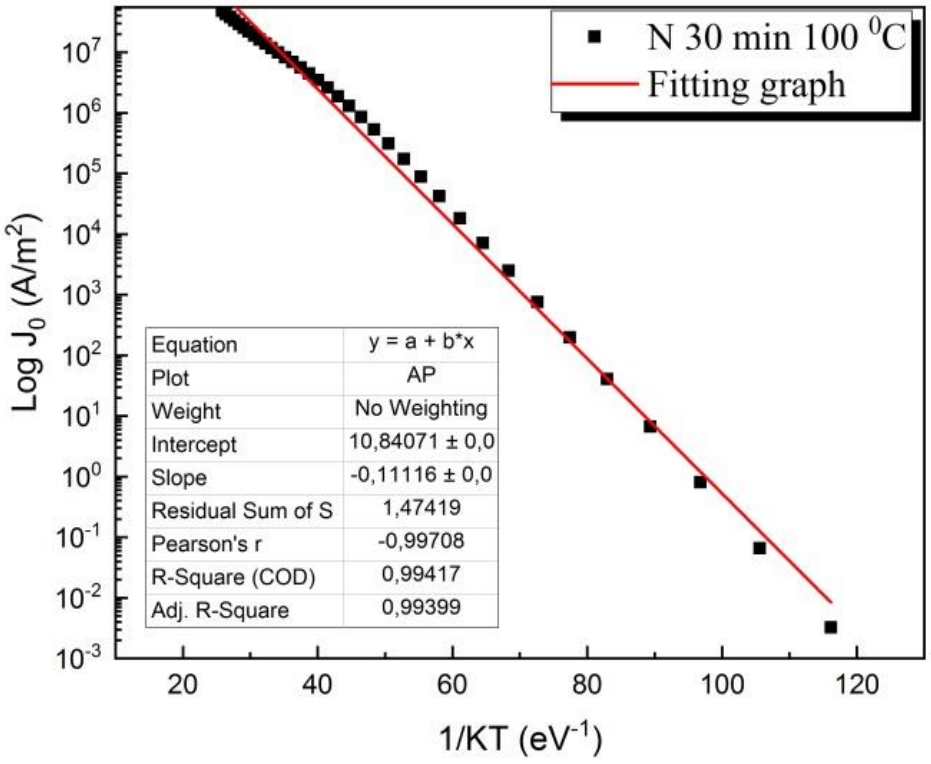

Figure 4. An example ofN30min sample illustrating fitting procedure to determine the activation energy of the samples.

4.2. Intrinsic nc-Si:Hsamples

The intrinsic samples were deposited without any impurities during 3min and 30 min and their activation energies (E_a) are simulated and given in the Figure 5 here bellow.

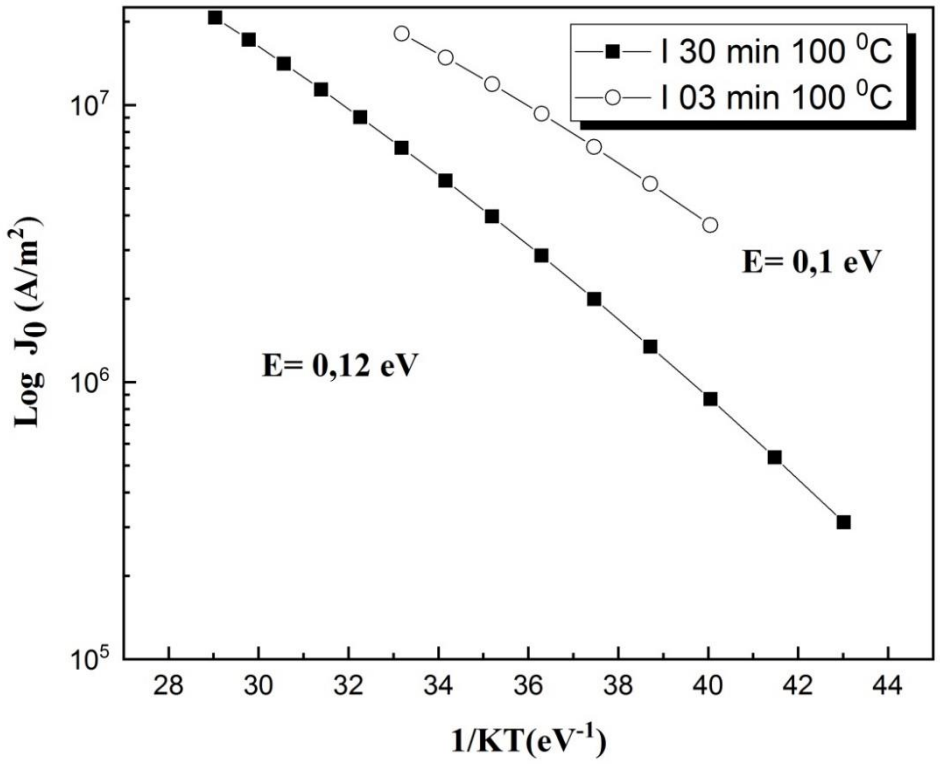

Figure 5. Simulated variation of $LogJ_0(T)$as a function of the inverse of KT, in temperature range 270-400 K obtained for intrinsic silicon thin films deposited at 3min and 30 min T = 100 °C.

We clearly see that both have small values of E_a. The only explanation of the one fabricated at 3 min could be the presence of defects and exterior atoms called impurities like oxygen which make from this material as n doped that is why its E_a is very weak.

It is possible, however, to modify the conductivity over many orders of magnitude by introducing even small concentrations impurities into the semiconductors. To increase the electron density in our samples an impurity such as phosphorus P is substituted for some of the Si atoms. Four electrons from each P atom go into bonding states with surrounding Si atoms but fifth is loosely bonded and can easily be excited in the conduction band [24].These P impurity sites are called donors since they donate electrons to the conduction band.

Similarly, the introduction of trivalent impurity such as boron B will introduce localized states just above the valence band. These are called acceptors since they can accept an electron excited from the valence band. The resultant increase in hole density in the valence band can also be used to increase the conductivity.

4.3. n-doped nc-Si:H samples

As indicated in the experimental work, these samples were deposited using phosphorus impurities, during two different periods of time as the intrinsic ones.

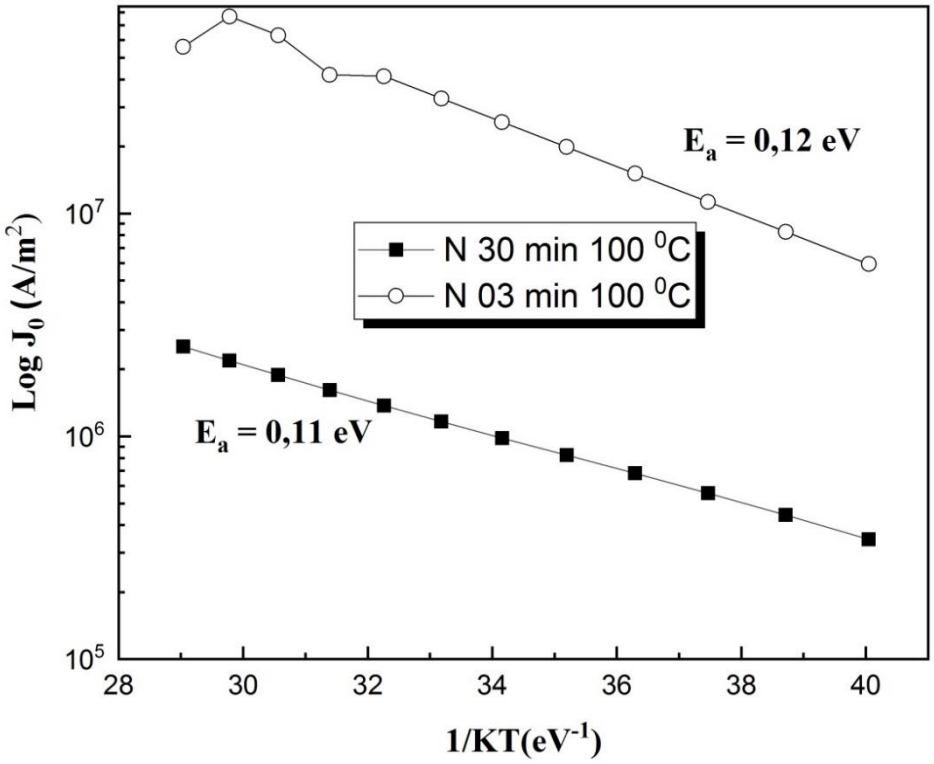

Figure 6. Simulated variation of *LogJ_0(T)* as a function of the inverse of KT, in temperature range 290-400 K obtained for n doped nanocrystalline silicon thin films deposited at 3 min and 30 min at T = 100°C.

In this kind of samples, the majority of carriers are the electrons and the calculated activation energy by simulation of both samples is around 0,1 eV which strongly means that the doping has a crucial role in effecting the electrical properties of the samples where it will be easy to generate electron hole pair using small energy.

4.4. p-doped nc-Si:H samples

As confirmed in the experimental work, these samples were madeusing boron impurities, during two different periods of time as the intrinsic ones.

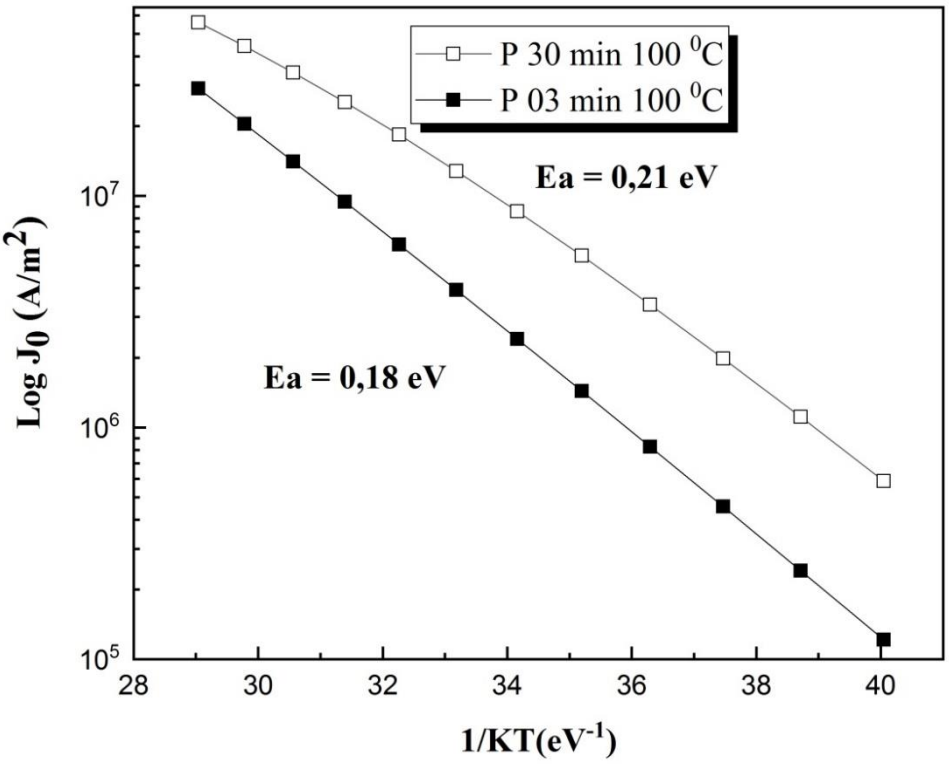

Figure 7. Simulated variation of $LogJ_0(T)$ as a function of the inverse of KT, in temperature range 290-400 K obtained for p doped nanocrystalline silicon thin films deposited at 3 min and 30 min at T = 100°C.

Boron impurities give to the doped material p characteristics where the majority of carriers are the holes and the calculated activation energy by simulation of both samples is around 0,2 eV which strongly means that the doping has an important effect on electrical properties of the samples where it will be easy to generate electron hole pair using small energy but still bigger than the one of n doped nanocrystalline silicon.It has also been pointed out that theincrease in conductivity could be caused by the increase in the portion of hopping conduction through defect states associated with the impurity atoms[23].

4.5. Hopping parameters

The activation energy for all samples was obtained between 0.1 and 0.2 eV. These values clearly differ from a typical recombination diode and must be explained by other mechanisms. [25]At low temperatures, electrons are able to surmount the lower barrier through tunnelling. Therefore, tunnelling will be the dominant transport mechanism of charge carriers ‘named Mott Variable Range Hopping (M-VRH)’ and the current is dominated by a tunnelling

process. This conductivity was first described by Mott for amorphous semiconductors, where the electrical conduction was shown to take place via the hopping of charge carriers from electrically active defect states (traps) to other traps with binding energies in the vicinity of Fermi level. In the Mott model, the density of states is assumed to be constant[25]. In addition,researchers studying different disordered material systems have also adopted the M-VRH model to describe the temperature dependent conductivity in their materials. This later conducted us to apply this model on our samples which can be considered as a material disordered[26].

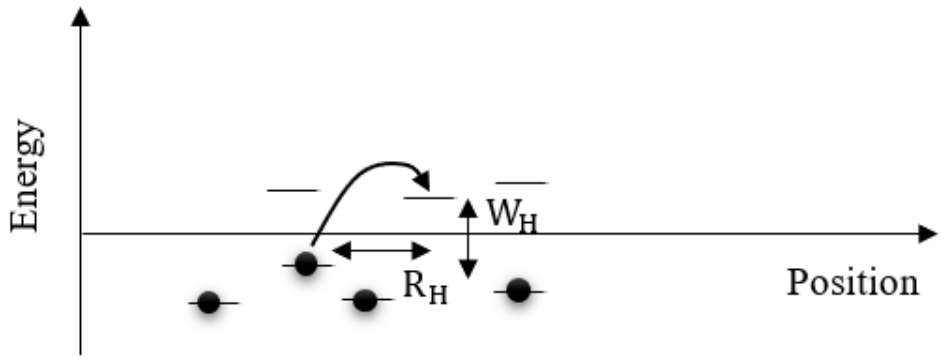

Figure 8. Diagram of the VRH hopping processes that account for electric transport in semiconductor materials for the region of low temperature. R_H and W_H indicate range and energy hopping activation [27][28].

In order to support this conclusion which suggests that the transport is dominated by M-VRH, we analysed the electrical characteristics at low temperature where[29]:

$$\sigma = \sigma_0 \, exp\left[-\left(\frac{T_0}{T}\right)^{1/4}\right] \qquad \text{(Eq.13)}$$

$$J_0 = J_{00} exp\left(\frac{Ea}{KT}\right) = J_{00} exp\left(\frac{Eg}{nKT}\right) \qquad \text{(Eq.14)}$$

$$J = J_0 exp\left[-\left(\frac{T_0}{T}\right)^{1/4}\right] \qquad \text{(Eq.15)}$$

Where :$Ea=\frac{Eg}{n}$, Ea: activation energy, Eg the gap energy , n is normally between 1 and 2

T_0 : disorder parameter

The conduction mechanism at low temperatures can be understood by plotting the $LogJ_0 \sim T^{-1/4}$ as illustrated in Figure 9.

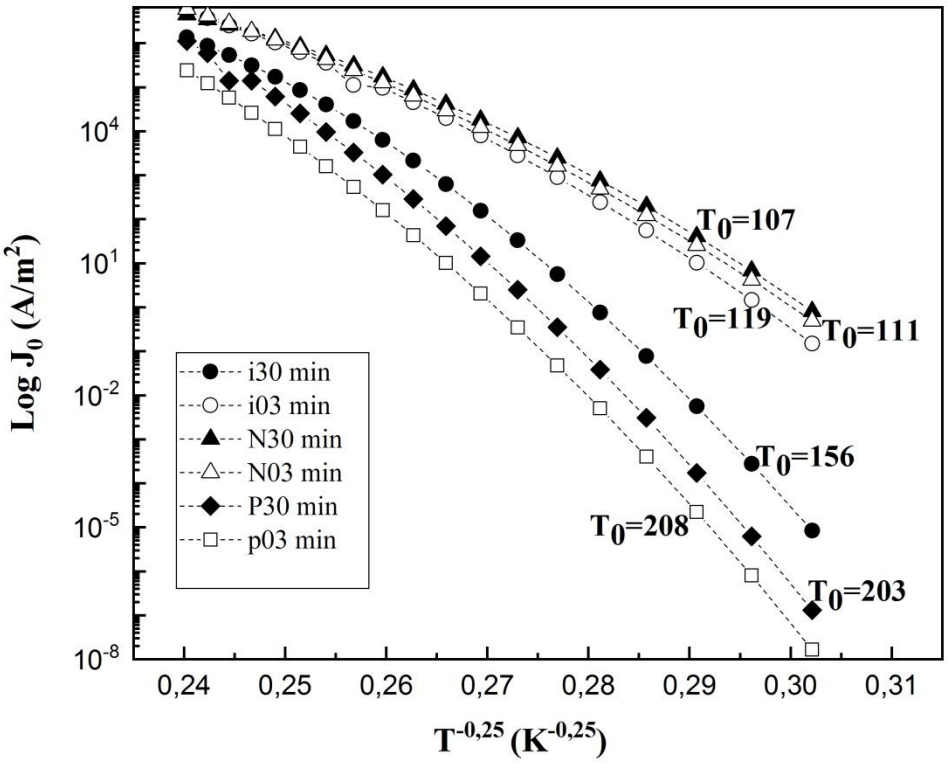

Figure 9. Thevariation of simulated *LogJ₀(T)* as a function of $T^{-0.25}$ for all the samples deposited during 3 min and 30 min at T = 100°C.

The linear fit reveals that the conduction is due to hopping between localized states. From the slope of $log\ J_0 \sim T^{-1/4}$, we obtained the disorder parameters T_0. This later gives the possibility to calculate the three parameters of the M-VRH mechanism.

4.5.1. N (E_F) parameter

This parameter represents the density of states at the Fermi level; it is calculated using the expression:

$$T_0 = 16\alpha^3/k\ \mathrm{N}(E_F) \qquad \text{(Eq.16)}$$

Where k is the Boltzmann constant and α is the inversereduction in length of localized wave functions $\alpha = 1/a_0$and a_0 is the Bohr radius[30].

Table 1. Summarizing simulated and experimental values of the disorder parameterEa, T_0, N(E_F)and LP.

Samples	**Ea(eV)**		**T_0(K)**		**N(E_F) (Ev^{-1} cm^{-3})**		**LP(Ev^{-1})**	
	Sim.	Exp.[1]	Sim.	Exp.[1]	Sim.	Exp.[1]	Sim.	Exp. [1]
I03MIN100	0.1	0.12	$2.00\ 10^{8}$	$2.12\ 10^{7}$	$1.9\ 10^{21}$	$8.76\ 10^{18}$	$2.8\ 10^{-4}$	$8.76\ 10^{-3}$
I30MIN100	0.12	0.18	$5.92\ 10^{8}$	$9.98\ 10^{7}$	6.610^{20}	$1.86\ 10^{18}$	$9.8\ 10^{-5}$	$1.86\ 10^{-3}$
N03MIN100	0.12	0.12	$1.51\ 10^{8}$	$2.24\ 10^{7}$	2.610^{21}	$8.29\ 10^{18}$	$3.8\ 10^{-4}$	$8.29\ 10^{-3}$
N30MIN100	0.11	0.14	$1.31\ 10^{8}$	$1.46\ 10^{5}$	$3.0\ 10^{21}$	$1.27\ 10^{21}$	$4.4\ 10^{-4}$	$1.27\ 10^{-3}$
P03MIN100	0.18	0.11	$1.87\ 10^{9}$	$1.30\ 10^{7}$	$2.1\ 10^{20}$	$1.43\ 10^{19}$	$3.1\ 10^{-5}$	$1.43\ 10^{-2}$
P30MIN100	0.21	0.20	$1.69\ 10^{9}$	$6.92\ 10^{7}$	2.310^{20}	$2.68\ 10^{18}$	$3.4\ 10^{-5}$	$2.86\ 10^{-3}$

In the table 1 the localization parameter is calculated using formula $LP=N(E_F)\alpha^{-3}$

The results presented in the table above strongly show a good agreement between the simulation and experimental values.All the samples have reasonable values of the hipping energy and length, besides their LP values is within the expected range [10^{-5} -10^{-1}] (eV^{-1}).

The plotted $N(E_F)$ vs $T_0^{0,25}$ as shown in the Figure 10 and the parameter values of the table 1, indicate that p doped samples and the intrinsic ones have small values of $N(E_F)$ whereas the n doped materials have big values.

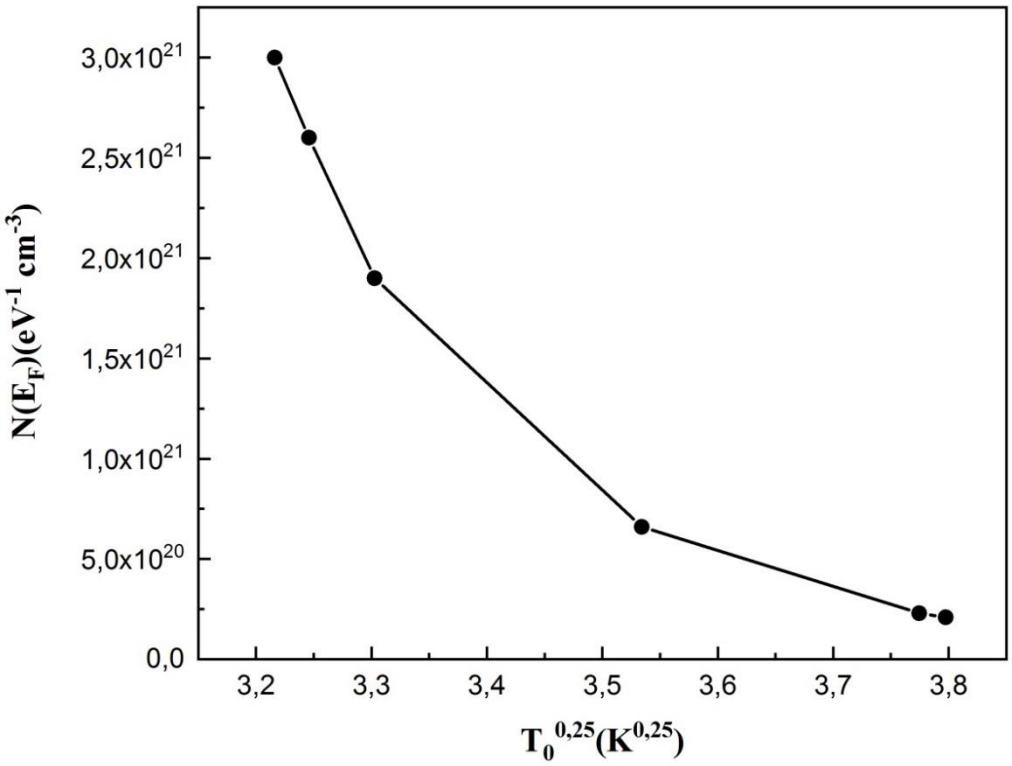

Figure 10. Variation, as a function of ($T_0^{0,25}$), of N(E_F) obtained for the samples. Continues line used to guide the eye.

The calculated values of the N(E_F) and T_0 can be conducted to deduce another important parameter of the hopping conduction model.

4.5.2. Range hoppingR_H

It is calculated using the following expression

$$R_h = \left[\frac{9}{8\alpha\pi K_B T \mathrm{N}(E_F)}\right]^{1/4} = \frac{3}{8\alpha}\left(\frac{T_0}{T}\right)^{1/4} \qquad \text{(Eq. 17)}$$

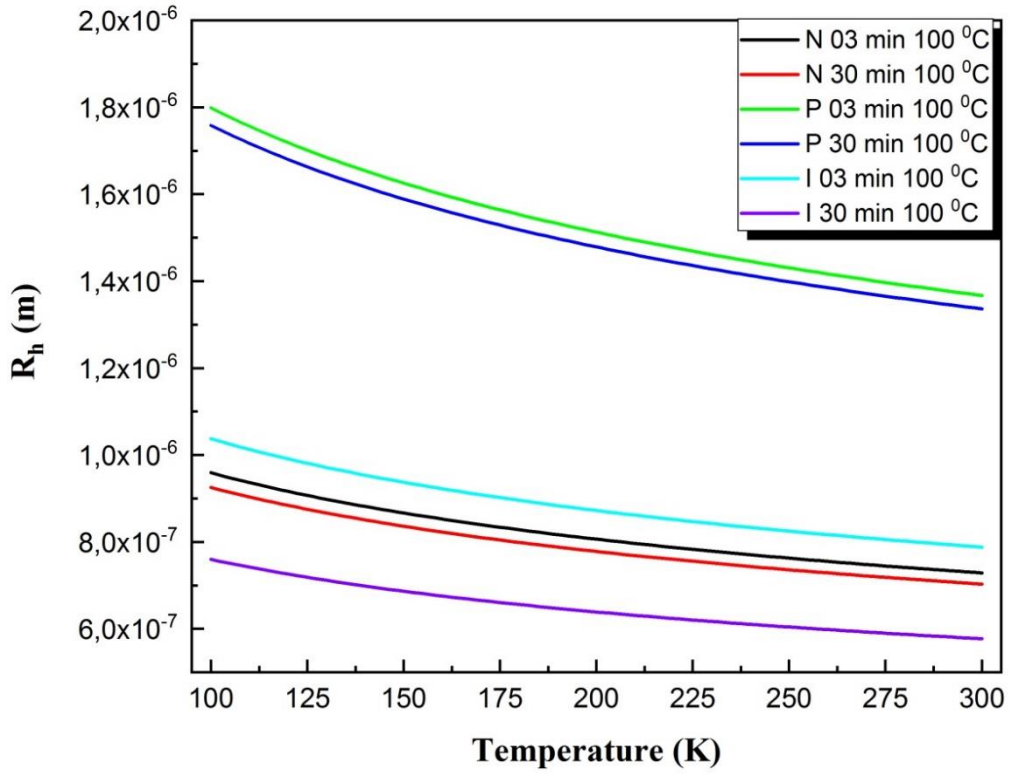

Figure 11. Variation, as a function of T, of the average hopping distance R_h.

In Figure 11, we plot the variation of R_h as a function of temperature. It is clear that the values of the average distance $R_h$are similar to those found in previous studies.

4.5.3. Energy range hoppingW_h

It can be calculated from the previous calculated parameters with using the expression 15,

$$W_h = \frac{3}{4\pi {R_h}^3 \mathrm{N}(E_F)} = K_B(T_0 T^3)^{1/4} \qquad \text{(Eq.18)}$$

The values of hopping energy W_h plotted in Figure 12 determined for our films are in good agreement with those previously obtained for films elaborated by other techniques.

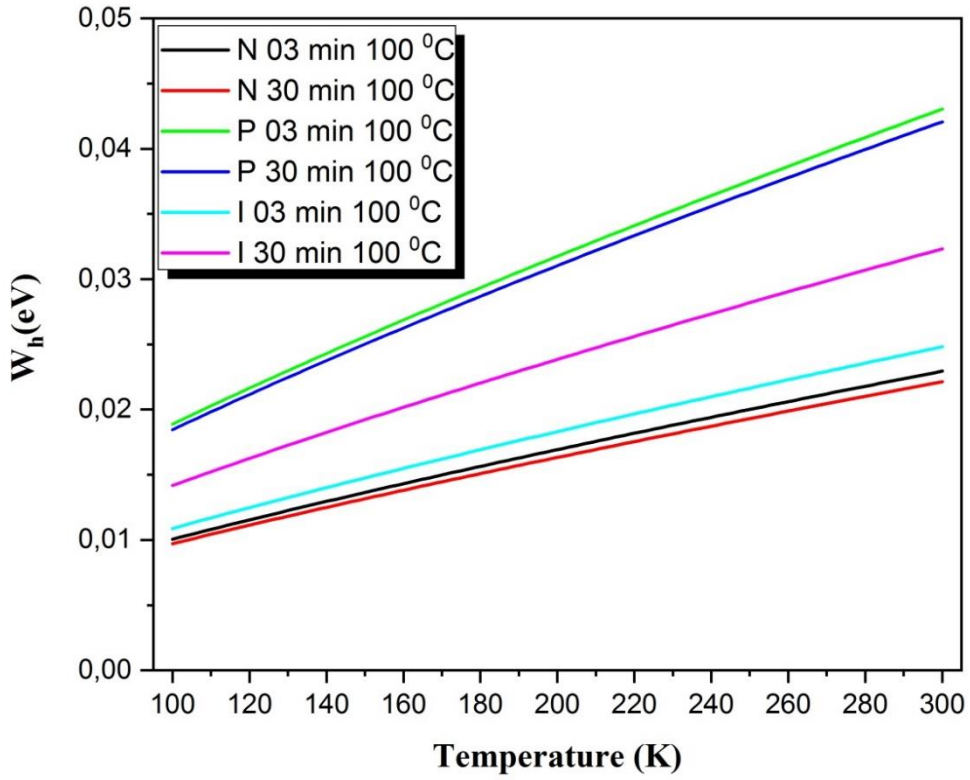

Figure 12. Variation, as a function of T, of the hopping energy deduced using the VRH model, for selected films deposited at 100°C, during 3 min and 30 min.

From the last three graphs and to conclude, it is strongly indicated that for all the investigated films, when N(E_F) increases, the distance R_h and the hopping energy W_h decrease. The explanation of this behavior is the increase of the crystallites sizes and the reduction of the defect density in grain boundaries, inducing a decrease of the distance and hopping energy between the crystallites.

Table 2. Summarizing simulated and experimental values of R_h and $W_h$obtained at room temperature

Samples	R_h(cm) at T = 300 K		W_h (eV) at T = 300 K	
	Simulation	Experimental[1]	Simulation	Experimental[1]
I03MIN100	$7.88\ 10^{-5}$	$2.83\ 10^{-7}$	0.024	0.106
I30MIN100	5.7710^{-5}	$4.17\ 10^{-7}$	0.032	0.155
N03MIN100	7.2810^{-5}	$2.87\ 10^{-7}$	0.023	0.107
N30MIN100	7.0310^{-5}	$8.17\ 10^{-8}$	0.022	0.030
P03MIN100	$1.36\ 10^{-4}$	$2.51\ 10^{-7}$	0.043	0.094
P30MIN100	1.3310^{-4}	$3.81\ 10^{-7}$	0.042	0.142

From Table 1 and 2 we can see that the intrinsic and doped samples have a values parameters including in the range values characteristics of the VRH transport and shown to be in agreement with the experimental values studied of other workers[32][1]for nanocrystalline silicon films.

4.6. Crystalline fraction effect on activation energy

We want to know the effect of crystalline fraction in the sample on the activation energy. To achieve this goal we took the sample (I30MIN100) with different X_c(from 10% till 90%). This effect is plotted in Figure 13 and the linear fit of data in this figure indicates the activation energy of this sample. The findings strongly confirm that when increasing crystalline fraction the activation energy deceases. This result confirms the crucial role of structure on the electrical properties of nc-Si:H studied in this project.

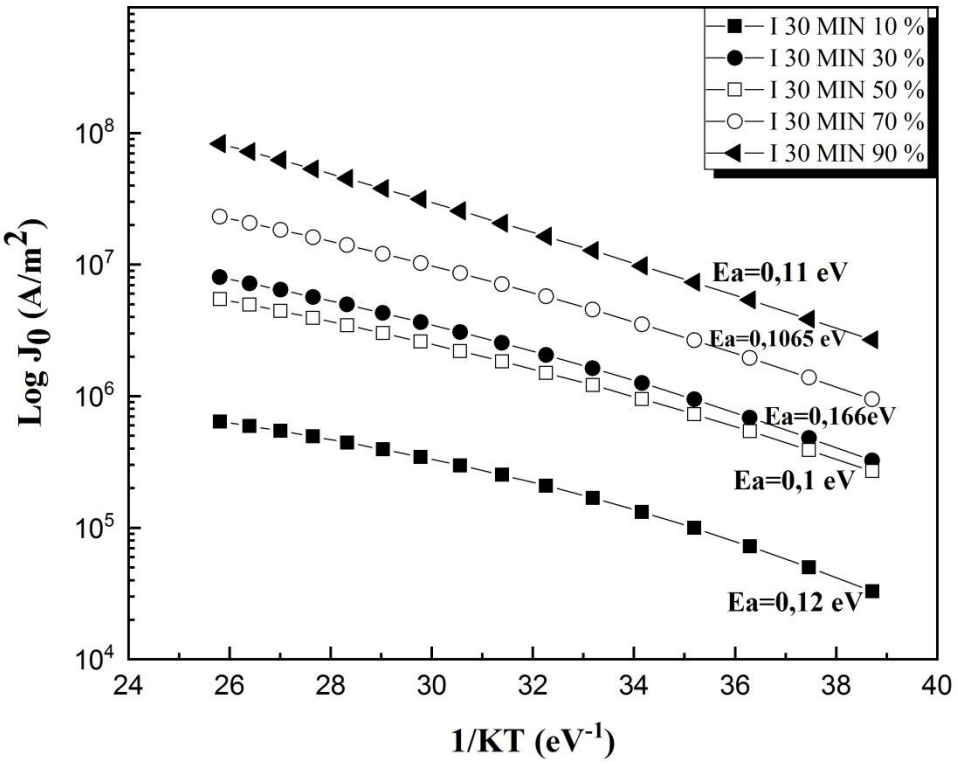

Figure 13. Simulated variation of $LogJ_0(T)$ as a function of the inverse of KT, in temperature range 300-450 K obtained for intrinsic nanocrystalline silicon thin film deposited at 30 min at T = 100°C taken with different crystalline fraction.

5.Conclusion

In this second part of our master project, we simulated using wxAMPS numerical tool the deposited nanocrystalline silicon samples at different times and a fixed temperature T = 100°C. Structures based models like GBT model has been proposed for our samples which states the carrier trapping at GB (amorphous regions) creates a potential barrier for charge transport which strongly influences the carrier conduction through the crystalline regions and disordered GB regions. The incorporation of P and B impurities into nc-Si results decrease of the density of localized states around the Fermi level.Our findings are clearly in good agreement with those obtained in the experimental work. The lower activationenergy valuesobtained, in experimental research, for the thin films grown during 3 min may be principally due to the presence ofdefects in grain boundaries as well as to oxygen atoms which might be incorporated in thethese films. In the low temperature range ($100 \leq T \leq 290$ K), the electrical conductivity mechanism is due to variable range hopping (VRH) in the localized states at the Fermi level, which is in fair agreement with Mott's conduction of

variable range hopping conduction. Thedifferent parameters such as the average hopping distance and hopping energy, determined bysimulation using this model, show a strong variation with temperature and are in good agreement withthose reported in the literature for films grown by other deposition techniques.

REFERENCES

[1] D. Benlakehal, A. Belfedal, Y. Bouizem, J. D. Sib, L. Chahed, et K. Zellama, « Electronic transport mechanism in intrinsic and doped nanocrystalline silicon films deposited by RF-magnetron sputtering at low temperature », *SuperlatticesMicrostruct.*, vol. 100, p. 228-236, déc. 2016, doi: 10.1016/j.spmi.2016.09.035.

[2] D. Senouci*et al.*, « Hydrogen related crystallization in intrinsic hydrogenated amorphous silicon films prepared by reactive radiofrequency magnetron sputtering at low temperature », *Thin Solid Films*, vol. 522, p. 186-192, nov. 2012, doi: 10.1016/j.tsf.2012.08.014.

[3] Y. Liu, Y. Sun, et A. Rockett, « A new simulation software of solar cells—wxAMPS », *Sol. Energy Mater. Sol. Cells*, vol. 98, p. 124-128, mars 2012, doi: 10.1016/j.solmat.2011.10.010.

[4] S. Yaşar, S. Kahraman, S. Çetinkaya, Ş. Apaydın, İ. Bilican, et İ. Uluer, « Numerical thickness optimization study of CIGS based solar cells with wxAMPS », *Optik*, vol. 127, nº 20, p. 8827-8835, oct. 2016, doi: 10.1016/j.ijleo.2016.06.094.

[5] Y. Liu, D. Heinzel, et A. Rockett, « A revised version of the AMPS simulation code », in *2010 35th IEEE Photovoltaic Specialists Conference*, Honolulu, HI, USA: IEEE, juin 2010, p. 001943-001947. doi: 10.1109/PVSC.2010.5616225.

[6] J. Smucker et J. Gong, « A comparative study on the band diagrams and efficiencies of silicon and perovskite solar cells using wxAMPS and AMPS-1D », *Sol. Energy*, vol. 228, p. 187-199, nov. 2021, doi: 10.1016/j.solener.2021.09.066.

[7] M. Burgelman, P. Nollet, et S. Degrave, « Modelling polycrystalline semiconductor solar cells », *Thin Solid Films*, vol. 361-362, p. 527-532, févr. 2000, doi: 10.1016/S0040-6090(99)00825-1.

[8] « A manual for AMPS-1D, http://www.ampsmodeling.org/latest.html#manual ».

[9] Z. A. K. Durraniet H. Ahmed, « NANOSILICON SINGLE-ELECTRON TRANSISTORS AND MEMORY », in *Nanosilicon*, Elsevier, 2008, p. 335-359. doi: 10.1016/B978-008044528-1.50011-7.

[10] D. Shan, M. Qian, Y. Ji, X. Jiang, J. Xu, et K. Chen, « The Change of Electronic Transport Behaviors by P and B Doping in Nano-Crystalline Silicon Films with Very High Conductivities », *Nanomaterials*, vol. 6, nº 12, p. 233, déc. 2016, doi: 10.3390/nano6120233.

[11] G. Y. Hu, R. F. O'Connell, Y. L. He, et M. B. Yu, « Electronic conductivity of hydrogenated nanocrystalline silicon films », *J. Appl. Phys.*, vol. 78, nº 6, p. 3945-3948, sept. 1995, doi: 10.1063/1.359914.

[12] J. Y. W. Seto, « The electrical properties of polycrystalline silicon films », *J. Appl. Phys.*, vol. 46, nº 12, p. 5247-5254, déc. 1975, doi: 10.1063/1.321593.

[13] P. G. Lecomber, G. Willeke, et W. E. Spear, « Some new results on transport and density of state distribution in glow discharge microcrystalline silicon », *J. Non-Cryst. Solids*, vol. 59-60, p. 795-798, déc. 1983, doi: 10.1016/0022-3093(83)90290-9.

[14] S. Tripathi, N. Venkataramani, R. O. Dusane, et B. Schroeder, « One-dimensional simulation study of microcrystalline silicon thin films for solar cell and thin film transistor applications using AMPS-1D », *Thin Solid Films*, vol. 501, nº 1-2, p. 295-298, avr. 2006, doi: 10.1016/j.tsf.2005.07.199.

[15] J. Kanicki, Éd.,*Amorphous and microcrystalline semiconductor devices*. in v. 2: The Artech House materials science library. Boston: Artech House, 1991.

[16] AnsgarJ¨ungel, « Transport Equations for semiconductors », Universit¨at Mainz.

[17] S. S. Hegeduset W. N. Shafarman, « Thin-film solar cells: device measurements and analysis », *Prog. Photovolt. Res. Appl.*, vol. 12, nº 23, p. 155-176, mars 2004, doi: 10.1002/pip.518.

[18] B. Yan, G. Yue, J. Yang, et S. Guha, « On the bandgap of hydrogenated nanocrystalline silicon intrinsic materials used in thin film silicon solar cells », *Sol. Energy Mater. Sol. Cells*, vol. 111, p. 90-96, avr. 2013, doi: 10.1016/j.solmat.2012.12.038.

[19] M. Chahi, A. Bouhekka, J. D. Sib, A. Kebab, Y. Bouizem, et L. Chahed, « Optoelectronic properties simulation of hydrogenated microcrystalline silicon Schottky diode », *Phys. Status Solidi C*, vol. 7, nº 3-4, p. 640-645, avr. 2010, doi: 10.1002/pssc.200982691.

[20] W. Fuhs, « Recombination and transport through localized states in hydrogenated amorphous and microcrystalline silicon », *J. Non-Cryst. Solids*, vol. 354, nº 19-25, p. 2067-2078, mai 2008, doi: 10.1016/j.jnoncrysol.2007.09.008.

[21] C. G. Van De Walle, « Band discontinuities at heterojunctions between crystalline and amorphous silicon », *J. Vac. Sci. Technol. B Microelectron. NanometerStruct.*, vol. 13, nº 4, p. 1635, juill. 1995, doi: 10.1116/1.587870.

[22] F. Montalvo-Galicia, M. T. Sanz-Pascual, P. Rosales-Quintero, et M. Moreno-Moreno, « Solar Cell Parameter Extraction Method from Illumination and Dark I-V Characteristics », *Nanomaterials*, vol. 12, nº 12, p. 1955, juin 2022, doi: 10.3390/nano12121955.

[23] M. A. Majeed Khan, M. Zulfequar, et M. Husain, « Electrical conduction mechanism in amorphous Se80In20−xPbx films », *Curr. Appl. Phys.*, vol. 2, nº 5, p. 401-406, oct. 2002, doi: 10.1016/S1567-1739(02)00148-7.

[24] P. G. Le Comber, « Electrical conduction in amorphous semiconductors », 1979.

[25] N. F. Mott, E. A. Davis, et R. A. Street, « States in the gap and recombination in amorphous semiconductors », *Philos. Mag.*, vol. 32, nº 5, p. 961-996, nov. 1975, doi: 10.1080/14786437508221667.

[26] KiranShrestha, « Electrical conduction mechanisms in the disordered material system p-type hydrogenated amorphous silicon », University of North Texas10.11144/Javeriana.SC19-2.phmd, 2014.

[27] A. Dussanet F. Mesa, « Procesos hopping a través del modelodifusional en materialesnanocristalinosusadosparaaplicacionesfotovoltaicas », *Univ. Sci.*, vol. 19, nº 2, p. 107-113, mars 2014, doi: 10.11144/Javeriana.SC19-2.phmd.

[28] M. A. Rafiq, « Carrier transport mechanisms in semiconductor nanostructures and devices », *J. Semicond.*, vol. 39, nº 6, p. 061002, juin 2018, doi: 10.1088/1674-4926/39/6/061002.

[29] B. Yan, G. Yue, J. Yang, et S. Guha, « On the bandgap of hydrogenated nanocrystalline silicon intrinsic materials used in thin film silicon solar cells », *Sol. Energy Mater. Sol. Cells*, vol. 111, p. 90-96, avr. 2013, doi: 10.1016/j.solmat.2012.12.038.

[30] A. K. Sharma et P. J. Reddy, « Electrical properties of amorphous and crystalline InSb and InAs thin films », *J. Non-Cryst. Solids*, vol. 41, nº 1, p. 13-30, sept. 1980, doi: 10.1016/0022-3093(80)90187-8.

[31] D. Benlakehal, A. Belfedal, Y. Bouizem, J. D. Sib, L. Chahed, et K. Zellama, « Electronic transport mechanism in intrinsic and doped nanocrystalline silicon films deposited by RF-magnetron sputtering at low temperature », *SuperlatticesMicrostruct.*, vol. 100, p. 228-236, déc. 2016, doi: 10.1016/j.spmi.2016.09.035.

[32] S. B. Concariet R. H. Buitrago, « Hopping mechanism of electric transport in intrinsic and p-doped nanocrystalline silicon thin films », *J. Non-Cryst. Solids*, vol. 338-340, p. 331-335, juin 2004, doi: 10.1016/j.jnoncrysol.2004.02.067.

General Conclusion and Perspectives

In this project, we were interested in studying and understanding, by simulation method; using the wxAMPS program the electrical properties due to light absorption by the microcrystalline silicon used as an active layer in some solar cells applications.

It was early reported in the first part of this manuscript the most important notions that allow the reader to clearly follow the document structure. The principles of solar cells and their corresponding structures and how light can be absorbed was discussed at the very beginning of the first chapter. After that the different structures of silicon and the transport mechanism with some theoretical models were presented to finish by some general definitions about heterojunctions.

In second chapter, it was indicated the simulation part and the results to understand the variation of some electrical properties especially the activation energy of intrinsic, n doped and p doped microcrystalline silicon thin films used as active layers in the solar cells. Doping increases light absorption probability in the active material. We found that the activation energy for doped layers is very low (less than 0,2 eV) compared to intrinsic layers.

It was strongly demonstrated that doping plays a crucial role in light absorption because changing the structure composition of the material will positively change the conductivity in dark. This increases light absorption into the bulk of active layer and thus the generation of electron hole pair should be increased.

The structure of the active layer is considered as one of the most important things that can change the light absorption in the cell. For this reason doping this layer was investigated in the second chapter. It was very clear from the given result that the cell made by μc-Si:H has lower activation energy compared to other ones. This behavior was explained by the difference in both structures where dangling bonds and defects in general plus the density of the material with the presence of impurities of boron or phosphorus affect strongly the light absorption and thus the conductivity induced.

As perspectives, the texturing of the surface of solar cell based on μc-Si:H as active material can be controlled by other important factors and this strongly enhance the light absorption thus the conductivity in the of the material. Due to the enormous applications of this study, we mention that improving this research in the future is a key factor to enhance light absorption. A lot of geometrical schemes were done by others however it is still not really well understood so proposing for example a combination at the same surface between

texturing and gratings can give more interesting results plus another idea using surface texturing in one side and gratings in the second side would be also a solution for light trapping. Injecting another structure completely different from crystalline and amorphous ones still a good idea like putting microcrystalline amorphous silicon (a-Si:H). In this case the small crystallites in this material can increase the light absorption probability.